Master´s Thesis

Development of Conductive Polymer Composites for the Material Extrusion of Dielectric Elastomer Actuators

From

Thomas Steinert, BSc.

Chair: Univ.-Prof. Dipl.-Ing. Dr.mont. Clemens Holzer
Leoben, August 2022

Declaration of Originality

I declare in lieu of oath, that I wrote this thesis and performed the associated research myself, using only literature cited in this volume.

Date	Signature

Acknowledgement

First of all, I would like to thank my supervising professor Univ.-Prof.- Dipl.-Ing. Dr.mont. Clemens Holzer. In addition, I would like to extend my gratitude to Dipl.-Ing. Stephan Schuschnigg and Ivan Raguž, MSc. for their correction and supportive work.

In implementing practical work for my thesis, I am grateful to Franz Bauer, Andrea Eder, Philipp Huber, Gerald Meier and Idria Tributsch.

Last but not least, my thesis would not have been completed without my Iris' support and motivation and as well big thanks to my parents.

Abstract

The research in actuators for special operations has strongly increased in the last decades and gathered high attention. To fulfil different requirements, actuators appear in many different variations. Lately the potential of Dielectric Elastomer Actuators (DEAs) has shown promising results.

A key objective of the study was to improve the conductivity of the electrode materials for DEAs with the same flexibility as commercially available materials. Within the COMET-Modul Chemitecture the research was supported in corporation with the Polymer Competence Center Leoben (PCCL) GmbH. As an additive manufacturing process, material extrusion was used to manufacture the DEAs.

Silver coated carbon fibres were determined to be the most promising filler type in this application by pre-tests. The chosen matrix was a thermoplastic elastomer (TPE)-type from the company BASF. Conductive Polymer Composites (CPCs) in the form of filaments were produced using different filler contents, and material qualification was achieved by tensile tests, microscopy, and electrical resistance measurements. Based on the first results using pure silver coated carbon fibres as filler, these electrodes performed better than the reference materials.

Compared to the reference, the CPC with 15 vol.% silver coated carbon fibres achieved the same displacement of 110 % with a voltage of 2.8 kV (reference material: 5.4 kV). This meant that half as much voltage was needed to achieve the same displacement. For the resistance measurement an impulse of 2 kV was needed though to achieve conductivity. For the actuators, however, that was not a problem, as they were powered by higher voltages (> 2 kV).

Being used as actuators as well, the electrodes were improved so that they could also be used in heating applications at low voltages (< 1 kV). Even though the improved CPCs had a better electrical conductivity, their additive manufacturing proved to be quite challenging. This was caused by the electrically conductive fillers, which also increased thermal conductivity. As a result, the produced filaments could not be printed since they softened too early in the printer and were no longer extrudable.

In order to counteract this problem, a different matrix was used. The TPE matrix was replaced by a conductive matrix (TPE + special carbon structure) to reduce the thermal conductivity. Neither of these methods worked, as the material was still too soft and the conveying system in the printer was too abrasive for the filament.

In conclusion, the improved electrodes for actuators achieved the in advance set goal, but the developed materials could not be used for heating.

Kurzfassung

Die Forschung auf dem Gebiet der Aktuatoren für Spezialeinsätze hat in den letzten Jahrzehnten stark zugenommen und große Beachtung gefunden. Um den unterschiedlichen Anforderungen gerecht zu werden, werden Aktuatoren in vielen verschiedenen Varianten eingesetzt. In letzter Zeit hat das Potenzial dielektrischer Elastomer-Aktuatoren (DEAs) vielversprechende Ergebnisse gezeigt.

In dieser Arbeit wurde der Fokus auf die Materialentwicklung der Elektroden für DEAs gelegt, mit dem Ziel, dass das entwickelte Material, bei gleicher Elastizität eine bessere elektrische Leitung aufweist als das kommerziell erhältliche Material. Im Rahmen des COMET-Moduls Chemitecture wurde in Zusammenarbeit mit der Polymer Competence Center Leoben (PCCL) GmbH die Forschung unterstützt. Der additive Fertigungsprozess der Aktuatoren erfolgte mittels Materialextrusion.

Aufgrund von Vorversuchen erwiesen sich silberbeschichtete Kohlenstofffasern als die vielversprechendsten Füllstofftypen für diese Anwendung. Das gewählte Matrixmaterial war eine TPE-Type vom Hersteller BASF. Mit unterschiedlichen Füllgraden wurden Conductive Polymer Composites (CPCs) in Form von Filamenten hergestellt und mittels Zugversuchen, Mikroskopie und Messung des elektrischen Widerstands eine Materialqualifizierung vorgenommen. Die ersten Ergebnisse mit rein silberbeschichteten Carbonfasern als Füllstoff erwiesen sich als bessere Elektroden, verglichen mit dem Referenzmaterial.

Im Vergleich zur Referenzwurde mit dem CPC, welcher mit 15 vol.% silberbeschichteten Carbonfasern gefüllt war, die gleiche Verschiebung von 110 % bei einer Spannung von 2,8 kV erreicht (Referenzmaterial benötigte 5,4 kV). Somit wurde für die gleiche Verschiebung nur die Hälfte der Spannung benötigt. Bei der Messung des elektrischen Widerstandes war jedoch ein Impuls von 2 kV notwendig, um die elektrische Leitfähigkeit zu erhalten. Für die Aktuatoren war dies aber kein Problem, da diese bei höheren Spannungen (> 2 kV) betrieben werden.

Als weiterer Schritt wurden die Elektroden weiter verbessert, um sie auch im niedrigen Spannungsbereich (< 1 kV) als Heizungen zu verwenden. Es konnte zwar eine verbesserte elektrische Leitfähigkeit erreicht werden, aber die additive Fertigung der verbesserten CPCs erwies sich als schwierig, da sich mit den elektrisch leitfähigen Füllstoffen auch die Wärmeleitfähigkeit verbesserte. Dadurch waren die hergestellten Filamente nicht mehr druckbar, weil sie zu früh erweichten und somit nicht mehr extrudiert werden konnten.

Um diesem Problem entgegenzuwirken, wurde versucht die TPE-Matrix durch eine leitende Matrix (TPE + spezielle Carbon Struktur) zu ersetzen, um die Wärmeleitung zu verringern. Dies führte aber auch nicht zum Erfolg, da sich das Material als zu weich erwies und die Fördereinrichtung im Drucker das Filament abrieb.

Abschließend kann gesagt werden, dass das im Vorhinein gesetzte Ziel mit der Verbesserung der Elektroden für Aktuatoren erreicht wurde, jedoch für Heizungen die Materialien nicht einsetzbar waren.

Table of Contents

1 Introduction

Actuators move or control a mechanism or system by converting a signal into a mechanical movement. Restrictions such as weight, size, shape, cycle time, etc. have led to investigate them for specific applications [25].

Dielectric Elastomer Actuators (DEAs) are a promising new type of soft transducer consisting of a thin membrane made of an elastomer. This membrane is positioned between two electrodes where a voltage is applied. Due to this voltage the opposite charges of the electrodes produce an electrostatic force, which wants to squeeze the membrane. However, the electrodes are bonded to the membrane, which causes a variation in size [25, 30]. If a fourth layer is applied, the size variation can be transformed into a bending of the DEA.

Electrostatically activated elastomeric actuators reaching strains up to 215 % have been presented in 2000 by Pelrine et al. [27]. This was the signal for the launch of DEAs, which gathered quick attention worldwide [21, 25, 30].

DEAs are used in a wide field of applications ranging from mm-sized devices to meter-long blimps. Compared to traditional actuators, DEAs do not have the rigidity and can be used for completely different motion and systems, such as bioinspired techniques [30].

Since industrial robots are often rigid and designed to perform repetitive tasks perfectly, they are limited in their ability to adapt to their environment or change shape. In this case, for large deformations and manoeuvres through unstructured, constrained spaces soft robotics are needed, using bioinspired, muscle-like movements. No damage is caused or stress concentrations are generated by this movement. Electric active polymers are one kind of smart materials for soft robotics that change their shape in response to an electrical stimulus. Since this type of soft actuation simulates the properties of natural muscles, it is becoming increasingly popular [12].

Talking about the challenges of DEAs, it has to be considered, although there has been done much research in selection and optimization of the elastomers, that much less attention has been dedicated to the compliant electrodes of those devices. In addition to being thin enough, they must maintain their conductivity while following the large strains on the elastomer membrane. Carbon grease, carbon powder, and thin metallic films are the most commonly used electrode materials in literature. Carbon grease is inexpensive and easy to apply to most dielectric elastomers, two arguments for using it [12]. Furthermore, challenges of DEAs are the operation at low voltages, miniaturization, large manufacturability and integrated sensing [30].

To be precise, there is not always a need for electrodes, because electric charges can be sprayed directly on the elastomer. This technique brings its own pros and cons. A big advantage is the prevention of manufacturing complicate electrodes or losing the limitation of stiffness produced by the electrodes, which are often more rigid compared to the elastomer. However, removing the sprayed charge is quite difficult, whereas electrodes can be switched on and off easily, assumed they are conductive enough [30].

2 Theoretical Background

In this chapter the theoretical part of this work is explained and the most important aspects and results of other researches are highlighted.

2.1 Conductive Polymer Composites

The field of Conductive Polymer Composites (CPCs) is an interesting topic. Due to the demand for flexible and stretchable electronic devices, CPCs have gained a lot of attention over the last decades. Usually, polymers do not come with electric conductivity, but this property can be given from conductive fillers such as Carbon Black (CB), metallic powders or other fillers. Mostly applications with CB or carbon fibres (CF) are used, because of their tendency to form a conductive network regarding to their chain-like aggregate structure and lower prize compared to metal powders [7, 26, 39].

Why CPCs should be used is because of their simple fabrication, tuneable properties and scalability. CPCs compared to metallic conductors exhibit the advantages that they can be easily shaped, have a low density and are resistant to corrosion [26].

One drawback of the CPCs is that the polymer requires a high amount of fillers to achieve the desired electrical conductivity, which also can lead to a higher stiffness of the composite itself and increased costs. However, the morphology of the conductive part in the CPCs and the interaction between fillers and polymer matrix play a key role in the behaviour. The distribution of the conductive fillers in the matrix is dependent on different factors such as for example the affinity of filler and polymer, the interfacial tension between the components, the mixing technology, time and temperature [7, 26].

2.1.1 Percolation Phenomena

The percolation phenomena can be observed at many CPCs. It means that a small increase of conductive filler causes a significant high increase in the conductivity which has a S-shaped function as result, when the filler content versus the conductivity is plotted. The further increase of filler would just have a marginally effect (Figure 1). What happens, is that the filler dispersion is changed and a conductive network out of the fillers is formed. The point where the CPC is changing from an insulator to a conductor is called percolation threshold. There are several ways to decrease the percolation threshold to a lower filler content. For example, the use of additives, the optimization of the processing or the size, distribution and porosity of the filler. The conductivity of the CPC (σ_c) can be approximately described with Equation (1) [28].

$$\sigma_c \approx \sigma_f(\varphi - \varphi_c)^t, where\ \varphi > \varphi_c \quad (1)$$

σ_f is the conductivity of the filler, φ_c describes the percolation threshold, φ is the filler volume fraction and t describes the critical exponent which is dependent on the aspect ratio of the filler itself [28].

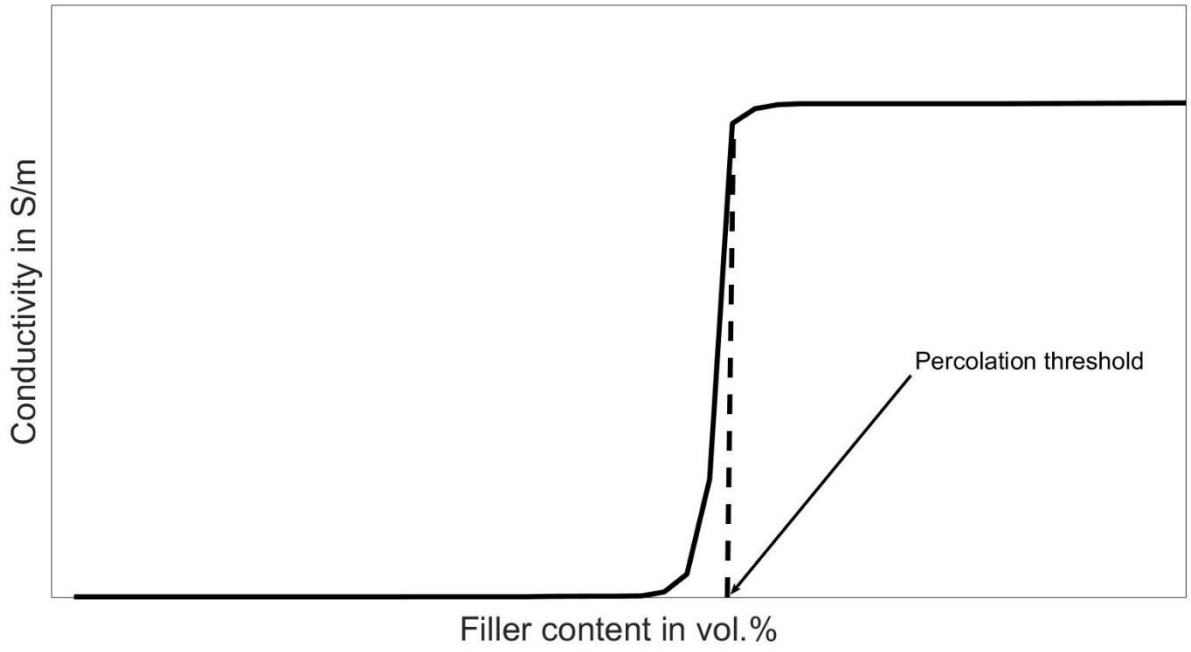

Figure 1: Schematic illustration of the percolation threshold

2.1.2 Mechanism of Electric Conduction

Different mechanisms of conduction can occur and depend on many factors, for example the types and concentration of fillers used in the CPC. Anyhow, the mechanism can be split up in two ways [26].

2.1.2.1 Adjacent

The first is that in insulating gaps of the size of a few nanometres between adjacent conductive areas, high field strength can be expected. For some conductive behaviours the internal field emission – a process of electron emission by the application of a strong electrical field – can be the reason. This mechanism is also called electron tunnelling [26].

2.1.2.2 Touching

The second reason for electric conduction is the formation of a conductive network which causes the flow of electrones, when an electrical field is applied. The reason of the conductive network is the physical contact of the conductive particles in the CPC, shown in Figure 2 [26].

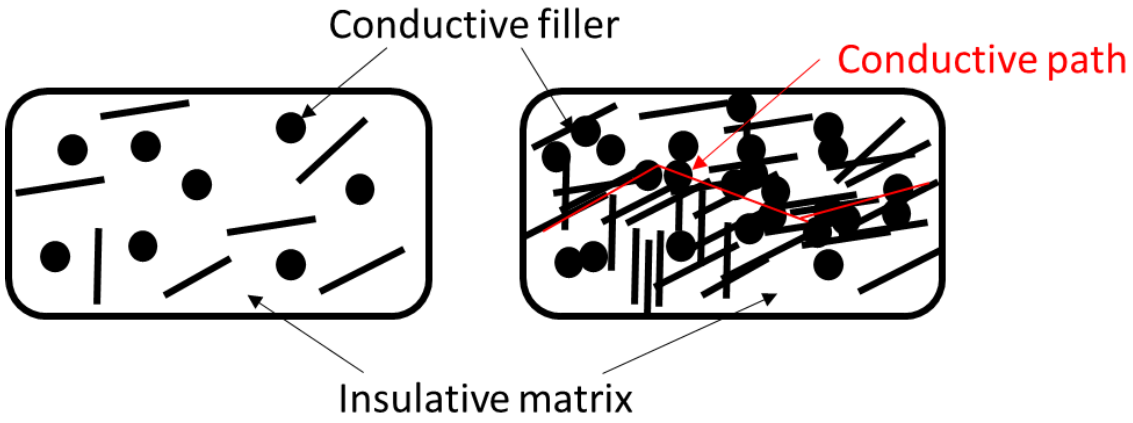

(a) (b)

Figure 2: Illustration of the filler distribution at (a) low and (b) high content forming a conductive path

2.1.3 Factors Influencing Conductive Properties

2.1.3.1 Processing Parameters

Talking about the processing parameters, the shear is considered in this paragraph, which has a significant influence on the conductive properties of the CPC. There are two considerable effects that on the one hand influence the properties positively, but on the other hand also can have negative influence. Those two effects are the dispersion of the particles throughout the matrix, which increases by longer and more intense shearing and the damage of the fillers due to shearing, which reduce the tendency to form conductive parts. This is why the parameters for mixing have to be taken into account to achieve a homogeneous dispersion of the fillers and not to damage the conductive particles [26, 36].

2.1.3.2 Polymer Matrix

A precise conclusion about the influence of the polymer cannot be done because of different reasons. Firstly, different polymers of the same kind may contain different additives that may result in different behaviours. Furthermore, the observation of different batches of the same material also may slightly deviate from each other. That is why it makes it hard to find a finite conclusion about the effect. However, one influence can be stated precise: the compatibility of the polymer with the filler. It was shown, that the better the compatibility the better the conductivity of the CPC. The reason for that is the better dispersion of the fillers and higher chance to form a conductive network. Whereas in polymers with lower compatibility it is more likely to form aggregates, which hinders the formation of chain structures [26].

2.1.3.3 Types of Fillers and Filler Concentration

Most of the conducting filler used for CPCs is CB. Carbon fibres also have the qualification being used in CPCs because of their high conductivity in polymers and lower need of filler

content. Research showed that carbon fibres provide conductivity – the transport of charges – over long distances, whereas CB improved the interfibre contacts.

Besides the structure, the size of the fillers also plays a main role. It was shown that smaller particles had a higher impact than bigger ones because of more formed conducting paths. The reason is the smaller gap between the conductive particles, which allows electrons to flow. For fibre shaped fillers it is not easy to control their size distribution because of the breakage happening during the mixing process mentioned before. Spherical parts are less affected and a wanted particle size distribution can be set [26].

2.1.3.4 Temperature

The influence of the temperature on the resistivity has been researched by many and can lead to positive, negative or neutral effects on the conductive properties, which change gradually with the change of temperature. A reason for an increase of the resistivity can be the different thermal expansion of the matrix and the fillers. Usually, the polymer has a higher thermal expansion than the fillers, which causes bigger gaps between the fillers and hinders the electrons to flow. A decrease of the resistivity may cause the flocculation of fillers leading to further conductive network. If increase and decrease of resistivity occur in the same amount, a neutral effect can be considered [26].

2.2 Fillers

Conductive Fillers are used to incorporate in the polymer – provided the matrix is not inherently conductive – to achieve conductive behaviour. A big variety of fillers occur in terms of size, structure, shape or material to name a few. As mentioned before the size of the fillers can have an effect on the conductivity, because the smaller the particles, the more they can interact with other conductive areas. The percolation threshold can also be reduced to smaller filler content when smaller particles are used [38]. As well as the size so does the aspect ratio, which describes the proportion of height and width of a particle, have an influence on the conductivity and percolation threshold. In comparison of fibres to spheres, fibres have a larger aspect ratio, because of the length related to their diameter, spheres show an aspect ratio of nearly one. This also takes influence on the critical exponent. The aspect ratio also has a positive effect on the tensile strength of the CPCs [26].

Silver

Compared to other metals, silver exhibits a high electrical conductivity, which makes it attractive for using it in CPCs. Another advantage is the relatively low tendency of oxidizing. However, due to the high costs and high amount of filler needed to reach the percolation threshold there has not been done a lot of research in the field of silver filled CPCs [26].

2.3 Thermoplastic Elastomer

Thermoplastic Elastomers (TPEs) consist of two-phase systems (hard and soft component), which behave when used as an elastomer and when processed at higher temperatures as a thermoplast. Those two phases have clearly different transition areas. The soft component is responsible for the elastomeric properties and connect the hard components, whereas the hard component forms the network, which is not permanent and can be detached. In contrast,

permanent cross-linked elastomers once vulcanized cannot be plasticized. There are two ways to produce TPEs: the block-copolymerization of hard and soft segments in the reactor or the mixing of incompatible polymer blends of thermoplasts and elastomers (Figure 3) [15, 17, 32].

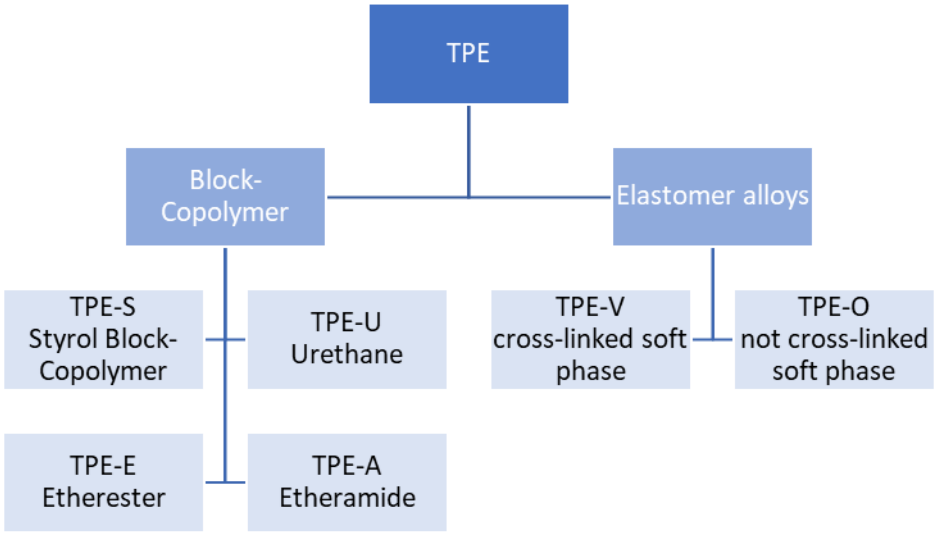

Figure 3: Classification of thermoplastic elastomers [15]

Thermoplastic Polyurethane

Thermoplastic Polyurethane (TPU) belongs to the group of thermoplastic elastomers and emerge via the copolymerization of polydiol (HO-R-OH, R is polyester or polyether), diisocyanate (O=C=N-R-N=C=O) and chain extenders in the form of low molecular diols or diamines. The polydiol and the diisocyanate build the soft phase, whereas the hard segment is formed by an excess of diisocynate reacting with the chain extender. Polyether types are more stable to hydrolysis than polyester types, but both are instable against acid and leach. The hardness of TPU lies between 70 Shore A to 80 Shore D [15, 17, 32].

2.4 Dielectric Elastomer Actuators

The growing interest in Dielectric Elastomer Actuators (DEAs) has emerged in the last decades. The reason is the potential in lightweight, easy production or emulation of natural muscles [6, 19].

DEAs consist of a thin membrane made of an elastomer. This membrane lies between two electrodes between which a voltage is applied. Figure 4 shows the basic construction of a DEA. Due to this voltage the membrane is squeezed by an electrostatic force (Maxwell stress). Equation (2) shows the strain s_z of the thickness z caused by this stress [30].

$$s_z = -\frac{\varepsilon_r * \varepsilon_0 * V^2}{z^2 * Y} \tag{2}$$

ε_r and ε_0 describe the relative and vacuum permittivity, V the applied voltage, z the thickness of the membrane and Y the Young's modulus of the elastomer. What can be read out of the equation is that the strain shows a quadratic dependence on the voltage, but as well on the thickness of the membrane. The quadratic dependence on the voltage can be seen in Figure 5

and additionally shows the maximally applicable electric field until it comes to a breakdown of the DEA [2, 30].

A big challenge for the DEAs are the driving voltages to reach the required electric field for operation. This is why research has been done for developing dielectric elastomers. Resulting in the fact that the Young's modulus Y and the dielectric constant of the elastomer ε have a significant influence on the strain response. It was shown that the ratio of ε/Y is directly proportional to the strain response (Equation (2))[20, 25, 34].

What has to be considered is that shortcuts precipitated by the high applied voltage and the resulting electric fields of the compliant electrodes can happen preferential at defects of the thin membrane. As a consequence, electric discharges happen, the membrane suffers heating and vaporization, and it leads to an inoperative DEA. To counteract or minimize a breakdown research is done in self-repairing or self-healing membranes, which can built a dielectric membrane again after breakdown [20, 25, 40].

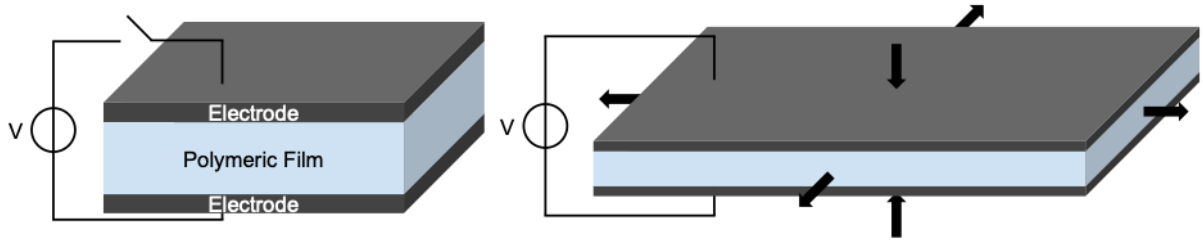

Figure 4: Basic construction and operation of a DEA [8]

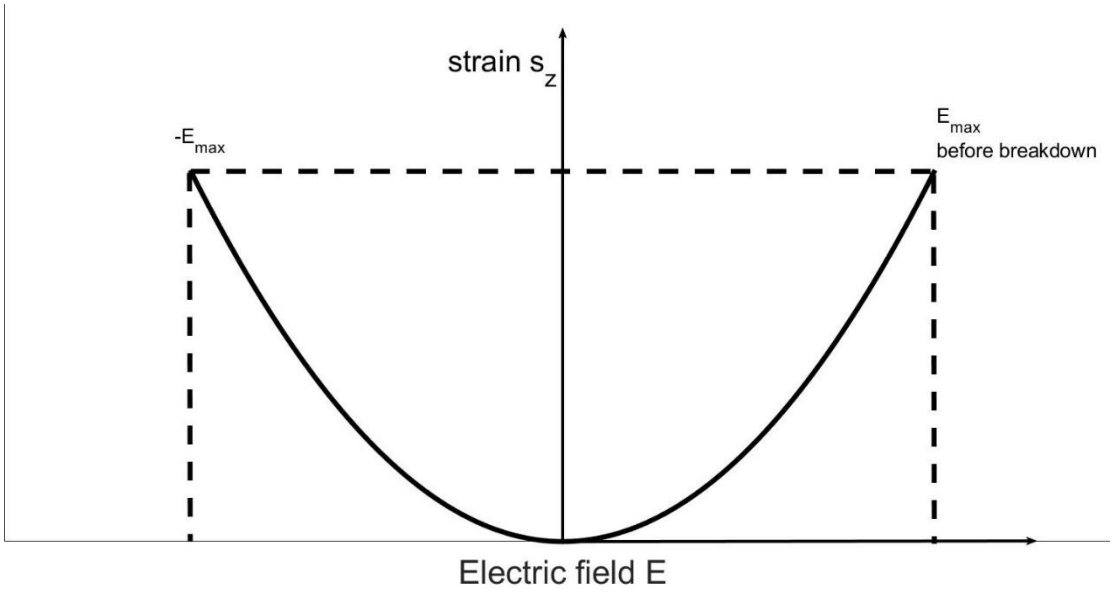

Figure 5: Strain versus applied electric field

2.4.1 Examples Artificial Muscles

Starting with the research in artificial muscles, DEAs have proved to be the most promising materials for such applications. Natural muscles are hard to be copied, because of the many different properties they have. However, DEAs compete with natural muscles in terms of high fracture toughness, large actuation strain and inherent vibration damping. Natural muscles are activated with chemical energy provided by food. In contrast, state of the art electro-magnetic motors come with a heavy pack of batteries, which have to be charged frequently. This reduces the energy density drastically, whereas natural muscles provide an energy density of aro und 150 J/kg. Secondly do electro-magnetic motors operate best at high rotational speed, which can be reduced significantly by using gearing system. Those systems increase the mass and reduce again the energy density. Moreover, natural muscles are able to absorb impact energy, which can be translated back into motion, while motors are not, rather they are noisy and generate more heat [2, 3, 13].

2.4.2 Transparent Application

DEAs used for transparency are inspired from the influence of the nature, where animals take the advantage of being transparent as a strategy for disguise and protection. There are some rules that have to be followed to achieve optimal results. Firstly, transpare nt material which does not absorb much light is required, secondly the thinner the better because of the reduced scattering of the light. Finally a flat surface hinders diffused reflection and improves the transparency [2, 23].

2.5 Additive Manufacturing

Additive Manufacturing (AM) is a term used for different processes of material processing. Generally, AM stands for the layer by layer construction of a 3D-part, which has been created before on a computer. An associated G-Code file is generated for the 3D-part, which is then processed by the 3D printer. In principle it is quite similar to a CNC-mill with the difference, that material is added and not removed. In addition, the part is divided (‘sliced’) in layers parallel to the building platform and converted to coordinates for the printer [18].

As early as 1980, Charles Hull was using what is today known as stereolithography to print with. With this technology a photo-curable liquid is hardened by ultraviolet light and the part is emerging out of the liquid polymer, quite fascinating to watch. Besides this technology, there are six other main processes related to AM. Table 1 shows all 7 methods for AM. Besides polymers other materials such as metals and ceramics have been able to be manufactured with AM technology [1, 18].

Table 1: Processes of additive manufacturing [5]

	An additive manufacturing process in which-
Material Extrusion	material is selectively dispensed through a nozzle or orifice
Material Jetting	droplets of build material are selectively deposited
Binder Jetting	a liquid bonding agent is selectively deposited to join powder materials
Sheet Lamination	sheets of material are bonded to form a part
Vat photopolymerization	liquid photopolymer in a vat is selectively cured by a light activated polymerization
Powder bed fusion	thermal energy selectively fuses regions of a powder bed
Direct energy deposition	focused thermal energy is used to fuse materials by melting as they are being deposited

2.5.1 Material Extrusion

Talking about Material Extrusion (MEX), it is an AM-process that places molten material by pushing it through a die or an orifice onto a surface, where it solidifies again. The Fused Filament Fabrication (FFF) uses a filament which is conveyed by an Extruder into a heating element, where it is molten and then pushed through a nozzle with a defined diameter (Figure 6) [5, 18].

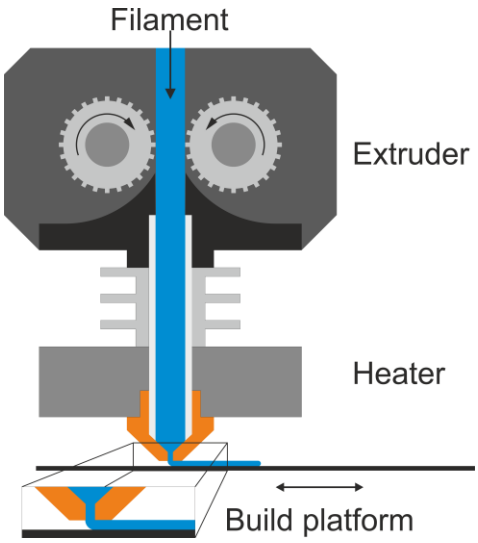

Figure 6: Basic construction of the MEX [14]

2.5.2 Future Developments

AM gave a rethinking in the economy in terms of the part designs and production. With the help of AM there is no need to design for production, but rather for function. In the beginnings of AM, the technology was used for prototypes. Today AM produced parts can replace existing parts in operation. To name an example, there have been cars that are made via AM technologies. Table 2 highlights the advantages of implementing an AM technology [1, 10].

Table 2: Advantages of additive manufacturing [10]

Use of less material	AM is known to build up the part layer by layer, whereas subtractive methods have to cut the parts, which leads to the fact that more material is required
Prototyping	Changes in the geometry of the part can be done way quicker by just printing prototypes
Integrated design	Parts suitable for the limited space and function can be produced more or less without any limitations in design
Lightweight parts	Lightweight parts help to reduce the total mass of the car and decrease mileage

2.5.3 Medical Application

A further big field for AM is the medical application, which includes the fabrication of surgical instruments, implants, protheses, bioprinting of tissues and organs and so on. The main goal of bioprinting is the reconstruction of a damaged tissue or organ with cells or bioactive materials. Living cells and/or biologically active molecules are seeded into a scaffold to regenerate or fix damaged tissues. Therefore the scaffold has to be highly porous to allow mass transfer and cell incorporation [1, 26].

2.6 Effect of Printing

2.6.1 Anisotropy

There has been done a lot of research on the mechanical properties influenced by the anisotropy caused by the AM process. However, there are limited results of the influence on the conductivity. It was shown that the conductivity can be dependent on the printing direction, due to the fact that the fillers get orientated during the printing process. One of the main factors, if the filler particles get orientated, is the aspect ratios of the parts. Moreover, it does not say that if the fillers get orientated there is a better conductivity, on the contrary it was shown that a better conductive network could be built, when the fillers lie more homogeneous and randomly dispersed in the polymer [26].

2.6.2 Printing Parameters

Influencing the conductivity, the most is probably the temperature of the nozzle. To ensure a constant extrusion of the material and avoid air gaps, the temperature has to be set correctly. The change of a few thicker layer to more thinner ones also has a positive effect on the conductivity [26].

2.6.3 Printing Nozzle

What is often neglected is the effect of the nozzle used in the printing process. CPCs always come with the effect of being quite abrasive to standard brass nozzles, which has a big influence over time, when the true nozzle diameter differs a lot from the assumed one. To overcome this problem nozzles with hardened steel or silicon carbide which are more wear

resistant are used. Secondly the shape of the nozzle has shown influence on the filler. Whereas converging nozzles had the impact to orient the fibres, diverging nozzles resulted in a randomization of the fillers in the polymer reducing the anisotropy. This effect was shown on tensile properties resulting in more isotropic behaviour. The impact on the conductivity has not been researched by now. Finally, what has to be considered is the size of the nozzle. It was shown that by increasing the diameter, the conductivity could be improved [26].

2.7 Microscopy

The use of a microscope is called into action when the resolution of the human eye is not sufficient. By using a microscope of this sort, significant statements can be made about a sample's morphology or surface. Morphology in polymers means the totality of structures reaching from few nm to 100 µm. Due to the fact that polymers nowadays do not just consist of pure polymer but also contain fillers the morphology also contains the structure of those fillers in the polymer [9].

2.7.1 Light Microscope

Via lenses objects get enlarged in the light microscope. Mostly, it is a system of two collecting lenses – the lens near the object and the ocular – where the total magnification is the result of the product of the two separate lenses magnifications. The maximum resolution of a light microscope is dependent on the wavelength of the light and cannot go under it. Figure 7 shows the main setup for a light microscope [9].

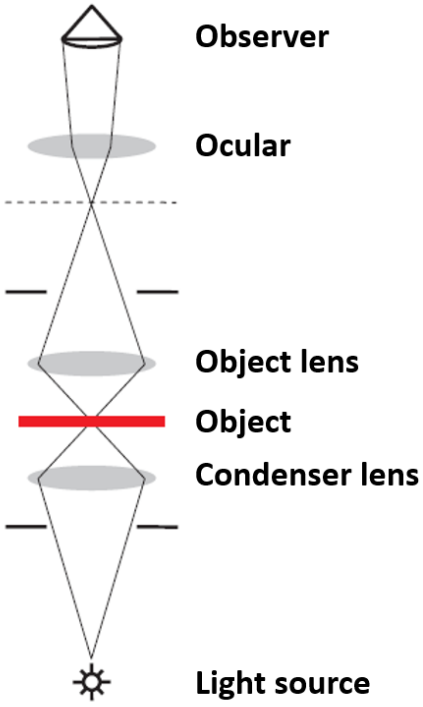

Figure 7: Setup of a light microscope [9]

2.7.2 Scanning Electron Beam Microscope

Differently to the light microscope, the scanning electron beam microscope (SEM) uses as its name implies an electron beam to enlarge the objects. The electron beam has a way smaller wavelength than the one from light which allows a higher resolution (ca. 1000x higher). Figure 8 shows the principle of the measurement. SE stands for secondary electrons and BSE for backscattered electrons, where both interact with the sample, get detected and are responsible for illustration of the surface [9, 16, 37].

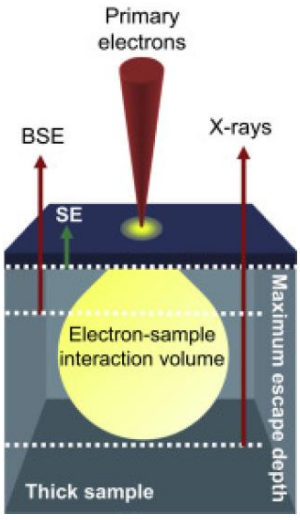

Figure 8: Principle of a SEM [16]

2.8 Electric Resistance

Most of the known technical polymers are not electrically conductive. This is because of their mostly unorganized structure. Therefore, polymers are used as insulation material in the electronic (e.g., cable insulation). In accordance with the Ohm's law the resistance is the relation of a voltage between two electrodes to the resulting current. Figure 9 shows the setup for measuring the resistance. Accordingly to specific standards (DIN IEC 60093, ISO 1853, DIN EN ISO 3915) the applied voltage is set and the resistance is measured [11].

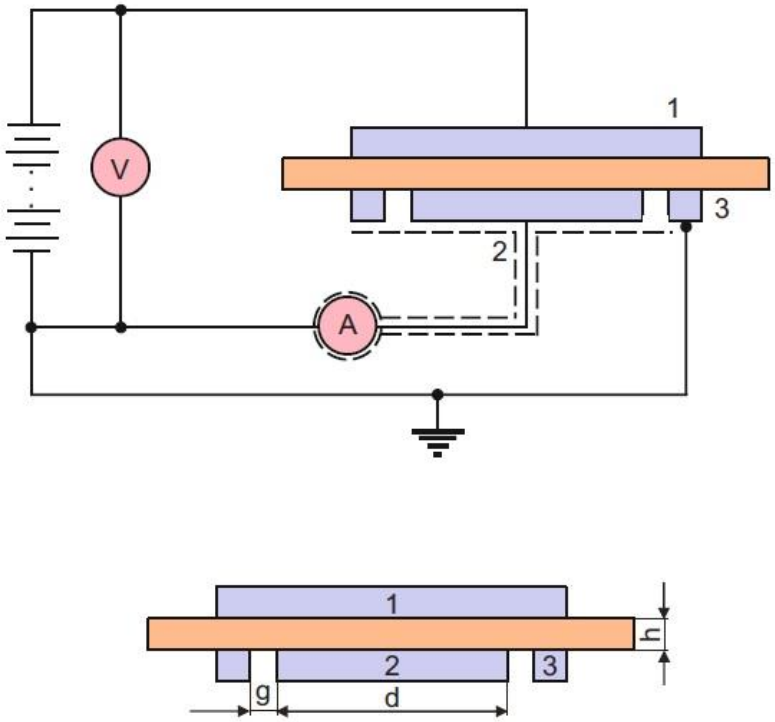

Figure 9: Measurement setup for resistance measuring [11]

2.9 Tensile Testing

In a tensile test the defined testing sample is clamped and treated with increasing tensile load until they break. The required force and the distance at the machinery is measured. Out of that the tensile modulus and breaking stress can be determined. The tensile modulus or Young's modulus (Y) is determined by the change of stress σ and strain ε (between 0.05 and 0.25 %) according to standard OENORM EN 527-2 (Equation (3)) [4, 11].

$$Y = \frac{\sigma_2(\varepsilon_2 = 0.25\%) - \sigma_1(\varepsilon_1 = 0.05\%)}{\varepsilon_2 - \varepsilon_1} = \frac{\Delta\sigma}{\Delta\varepsilon} \tag{3}$$

In contrast, the breaking stress is determined by the force per cross sectional area. Different stresses can be defined: for example, the breaking stress σ_b or the yield stress σ_y (Figure 10).

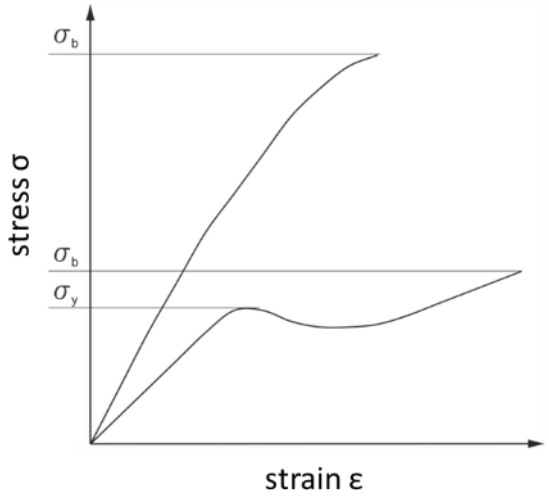

Figure 10: Schematic stress-strain-diagram of tensile tests

3 Experimental

A description of the practical parts and experiments that were conducted is presented in this chapter. The following examples display the abbreviations for the different CPCs for clarification and further understanding. The first abbreviation on the left stands for the CPCs only filled with carbon fibres (CF) with different volume fractions xx. CPCs filled with CF and glass spheres (GS) of different sizes and silver content xx/xx can be seen on the right. The employed fillers are shown in Table 3.

The carbon fibre has a nominal diameter of 30 µm and a silver coating of 30 vol.%. This would mean that the silver coating has a thickness of 2.928 µm. The glass spheres come in two sizes, the smaller one with a thickness of the coating with 0.252 µm and the bigger with 0.493 µm.

CPC_CF_xx-vol.% CPC_CF_xx-vol.%_GS_xx/xx_xx-vol.%

In order to compare and as a reference, a commercially available conductive filament was evaluated, and the results compared with those of the self-made filaments. The reference material was the Eel™ TPU 3D from Fenner Inc. (USA)

3.1 Materials and Formulations

In Table 3 the different types of fillers are shown. Table 4 shows the mechanical properties of the used TPE serving as matrix. The data sheets are added in the appendix.

Table 3: Employed conductive silver coated fillers from Kymera International (USA)

Ag/+	**Carbon fibre 30/30 fi**	**glass 5/25 s**	**glass 35/8 s**
Shape	fibres	spheres	
D50 value in µm	25-30	5-10	30-40
Ag-content in vol.%	28-32	23-26	7-9
Density in g/cm³	4.36	4.58	3.1

Table 4: Mechanical properties of Elastollan® 1170 A from BASF (Germany)

Density in g/cm³	1.08
Tensile Stress (Yield) in MPa	30
Shore Hardness (Shore A)	71
Processing (Melt) Temperature in °C	160 to 220

Due to pretests, the best conductive filament could have been achieved with the silver coated carbon fibres. That is why further kneading formulations were made only with carbon fibres. In order to increase conductivity and improve the contact between the fibres in the first CPCs

with carbon fibres, glass spheres were inserted among the fibres. A list of the kneading trials is shown in Table 5.

Table 5: Different formulations for CPCs

sample identifier content in vol. %	matrix (Elastollan® 1170 A)	Ag/Carbon fibre 30/30	Ag/Glass sphere 5/25	Ag/Glass sphere 35/8
CPC_CF_10-vol.%	90.0	10.0	-	-
CPC_CF_12.5-vol.%	87.5	12.5	-	-
CPC_CF_15-vol.%	85.0	15.0	-	-
CPC_CF_17.5-vol.%	82.5	17.5	-	-
CPC_CF_20-vol.%	80.0	20.0	-	-
CPC_CF_15-vol.% _GS_5/25_2.5-vol.%	82.5	15.0	2.5	-
CPC_CF_15-vol.% _GS_5/25_5.0-vol.%	80.0	15.0	5.0	-
CPC_CF_15-vol.% _GS_35/8_2.5-vol.%	82.5	15.0	-	2.5
CPC_CF_15-vol.% _GS_35/8_5.0-vol.%	80.0	15.0	-	5.0

Based on the following equations, the different volume contents and masses of the fillers and matrix material for kneading were determined. The volume of the kneader is in total 38 cm³ . In equation (4) the volume of the filler v_{f+s} is calculated, where v_p represents the volume of the matrix material and $vol.\%_{f+s}$ the desired volume percent of the fillers.

$$v_{f+s} = \frac{v_p * vol.\%_{f+s}}{(1 - vol.\%_{f+s})} \tag{4}$$

With equation (5) the required mass m was calculated out of the volume V and the density ρ.

$$m = \frac{V}{\rho} \tag{5}$$

3.2 Kneading

The Messkneter Plasticorder from Brabender GmbH & Co.KG (Germany) was used for the kneading trials. Table 6 shows the kneading settings and programme. Figure 11 illustrates the open kneading chamber after the mixing programme with a CPC, which was processed at the Institute of Polymer Processing.

Table 6: Settings and programme for kneading

Settings		
Total kneading time in min	30	
Temperature in °C	190	
Programme		
Time in min	Rotational Speed in rpm	Notes
0	15	½ of polymer
3		½ of filler
8		½ of polymer
11		½ of filler
11	60	turn up to 60 rpm after filling
30		mix till end of time

Figure 11: Open kneader chamber for mixing conductive polymer composites

3.3 High Pressure Capillary Rheometer

With the High Pressure Capillary Rheometer (HPCR) Rheograph 2002 from Göttfert Werkstoff-Prüfmaschinen GmbH (Germany) the filaments were produced with a downstream teflon-conveyer belt (GAL-25, Geppert-Band GmbH, Germany) again at the Institute of Polymer Processing. There were 1.75 millimetres of diameter and 30 millimetres of length in the used die. 190 °C was set as the temperature for the entire HPCR.

3.4 Microscopy

The microscope images were done at the PCCL with the Axioscope 7 MAT from Carl Zeiss Microscopy Deutschland GmbH (Germany).

3.5 Scanning Electron Beam Microscopy

With the Tescan Vega II from TESCAN (Czech Republic) the SEM images were made at the Institute of Materials Science and Testing of Polymers.

3.6 Tensile Testing

The tensile tests were done on the Zwick Roell universal testing machine from Zwick Roell GmbH & Co. KG (Germany) at the Institute of Materials Science and Testing of Polymers. For the Young's modulus the speed of the lifting beam was 1 mm/min. Rest of the measurement was performed at 50 mm/min. In contrast to the standards, no specified dog bone specimens were used, but the filaments with a diameter of 1.75 mm produced with the HPCR were tested.

3.7 Electrical Resistance

The filament resistance could not be measured with a simple multimeter. The setup had to be changed accordingly. In Figure 12 the measurement setup for the resistance is illustrated. This development allowed higher voltages to be used and filament gauges to be taken. It was necessary to calibrate the assembly with known ohmic resistance (Rv) values first. For different voltages, the drop-in voltage at the resistance was measured and curves were plotted after they were penetrated with a certain value of voltage. After calibration the resistances got replaced by the filaments and they got gauged for a distance of 20 cm (Figure 13). In the same way, the voltage drop was measured and the resistance was counted back from there.

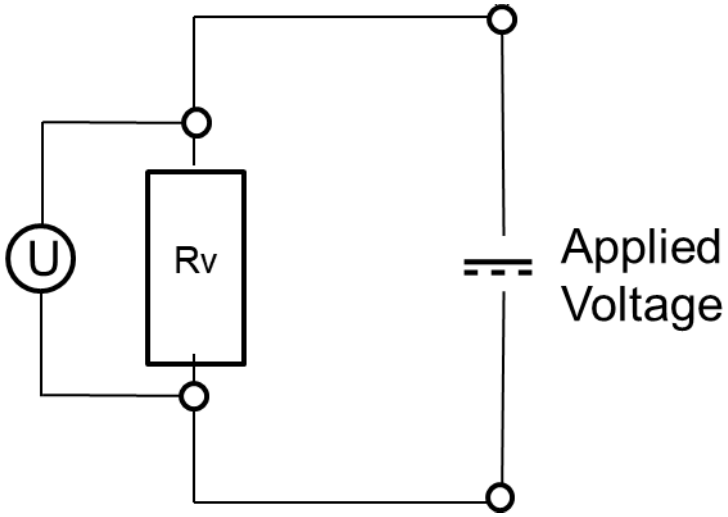

Figure 12: Setup for measuring voltage at different resistances R_V

Figure 13: Measuring device for the resistances of the filaments with a specific length of 20 cm

3.8 Material Extrusion

The passive component of the actuator was printed first, then the active part was placed on top of it. The main printer settings can be seen in Table 7. The used 3D Printer for the DEAs was the CreatBot F430 from Henan Suwei Electronic Technology Co. (China), a dual-extruder for material extrusion.

Table 7: Printer parameters for printing DEAs

Printer Parameters	
Build platform material	Glass
Build platform temperature in °C	45
Printing parameters for membrane and passive component (Extruder 1)	
Filament	NinjaFlex® TPU
Nozzle diameter in mm	0.3
Nozzle temperature in °C	250
Nozzle material	Brass
Infill	Rectilinear at ±45°
Thickness of first layer (passive component) in mm	0.1
Number of layers passive component	1
Printing speed of first layer in mm/s	20
Thickness of membrane layers in mm	0.05
Number of membrane layers	3
Printing speed of membrane layers in mm/s	20

Table 7 continued

Printing parameters for electrodes (Extruder 2)	
Filament	CPCs
Nozzle diameter in mm	0.6
Nozzle temperature in °C	220
Nozzle material	hardened steel
Infill	Rectilinear at 90°
Thickness of electrode layer in mm	0.05
Number of electrode layers per electrode	1
printing speed of electrode layers in mm/s	18

In Figure 14 the geometry of the DEA is visible consisting of 4 layers (passive layer, electrode 1, membrane and electrode 2). There are two ports on the left side for the cables that apply voltage for operation.

Figure 14: Geometry of Dielectric Elastomer Actuator

4 Results and Discussion

An analysis of the achieved results, as well as comparisons with literature that is relevant to this research area, is presented in this chapter. A direct discussion of the results is also included.

4.1 Kneader

Figure 15 shows a representative curve of the kneading process for a set time of 30 minutes. At the beginning of the experiment, the torque is observed to increase, as the polymer matrix and fillers are added. When the kneader is fully filled after 11 minutes, the rotation speed increases from 15 to 60 rpm, increasing the torque as well. From this point onwards, the torque decreases as the composite homogenies till the end of the mixing process and optimally would stabilize. The other curves of the torque versus time during the kneading process are listed in the appendix. As shown in Table 8, the torque at the end of the mixing time of 30 minutes can be determined for each CPC. Considering the kneader machinery and data recording is quite old and could be saved only on floppy disks, the values were read out using the implemented monitor and a deviation of 0.2 Nm was assumed for all measurements. The increased amount of colloidal interaction of the silver coated carbon fibres leads to the increase of the torque [31]. The spheres did not show this influence on the torque, only the size had an impact.

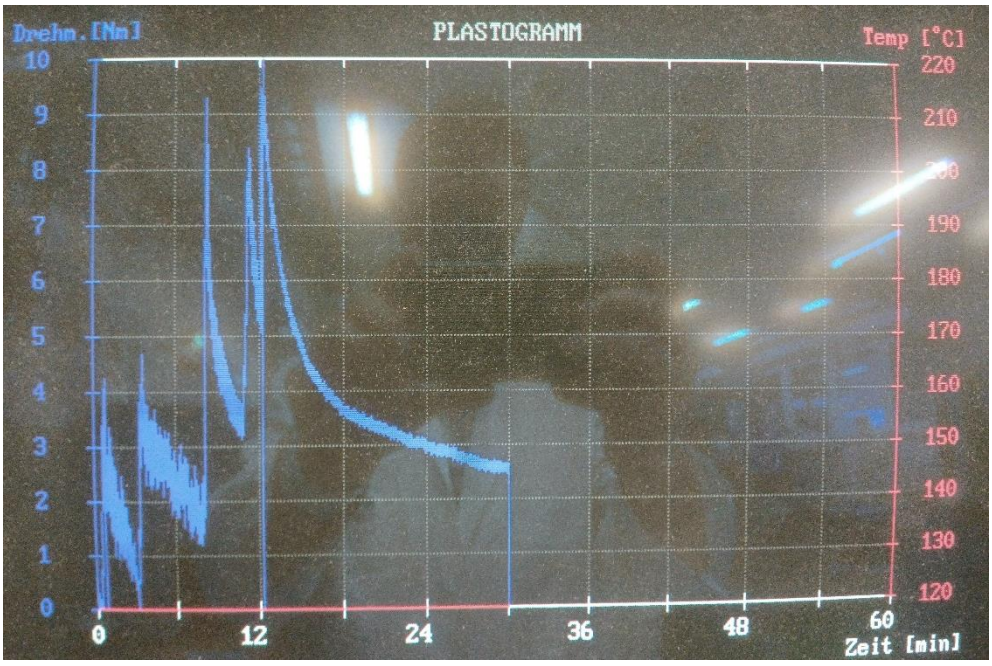

Figure 15: Representative curve of torque versus time for the kneading process (CPC_CF_15-vol.%)

Table 8: Torque after a mixing time of 30 min in the kneader for each CPC

sample identifier	torque at 30 min in Nm
CPC_CF_10-vol.%	2.1 ± 0.2
CPC_CF_12.5-vol.%	2.1 ± 0.2
CPC_CF_15-vol.%	2.5 ± 0.2
CPC_CF_17.5-vol.%	2.8 ± 0.2
CPC_CF_20-vol.%	3.0 ± 0.2
CPC_CF_15-vol.% _GS_5/25_2.5-vol.%	2.5 ± 0.2
CPC_CF_15-vol.% _GS_5/25_5.0-vol.%	2.5 ± 0.2
CPC_CF_15-vol.% _GS_35/8_2.5-vol.%	2.7 ± 0.2
CPC_CF_15-vol.% _GS_35/8_5.0-vol.%	2.7 ± 0.2

4.2 High Pressure Capillary Rheometer

The high-pressure capillary rheometer was used for extruding the filaments and during the process the pressure was recorded and plotted versus time. Those graphs are shown in the appendix. Table 9 shows the mean values and standard deviation of the pressures during constant extrusion of the separate CPC formulations. No significant influence of the filler content on the pressure could be detected.

Table 9: Mean value of the pressure at HPCR for each CPC

sample identifier	pressure in bar
CPC_CF_10-vol.%	44.5 ± 3.2
CPC_CF_12.5-vol.%	64.2 ± 1.3
CPC_CF_15-vol.%	65.1 ± 0.7
CPC_CF_17.5-vol.%	62.4 ± 1.4
CPC_CF_20-vol.%	65.3 ± 2.1
CPC_CF_15-vol.% _GS_5/25_2.5-vol.%	58.6 ± 4.8
CPC_CF_15-vol.% _GS_5/25_5.0-vol.%	56.4 ± 3.9
CPC_CF_15-vol.% _GS_35/8_2.5-vol.%	61.2 ± 1.6
CPC_CF_15-vol.% _GS_35/8_5.0-vol.%	66.8 ± 0.3

4.3 Microscopy

For the microscopy the filaments were cryo-fractured, which means that they were dived in liquid nitrogen and then quickly broken to have a clear structure of the fractured surface.

4.3.1 Light Microscope

The pictures were made with a polarization filter of 0 °. The settings of all light microscope is bright field and an enlargement of 100 times. Starting with the light microscopy the increasing infill and dispersion of the particles can be seen in Figure 16 to Figure 20 for the carbon fibre filled CPCs, reaching from 10 vol.% to 20 vol.% by steps of 2.5 vol%. Those figures were done with the light microscope with the intention to see, if there are agglomerations or if the fibres are evenly dispersed. The pictures show the latter case. The fibres that appear black have not lost their silver coating, it is just because of the polarization filter, which just let the reflection of the silver with an orientation of 0 ° pass.

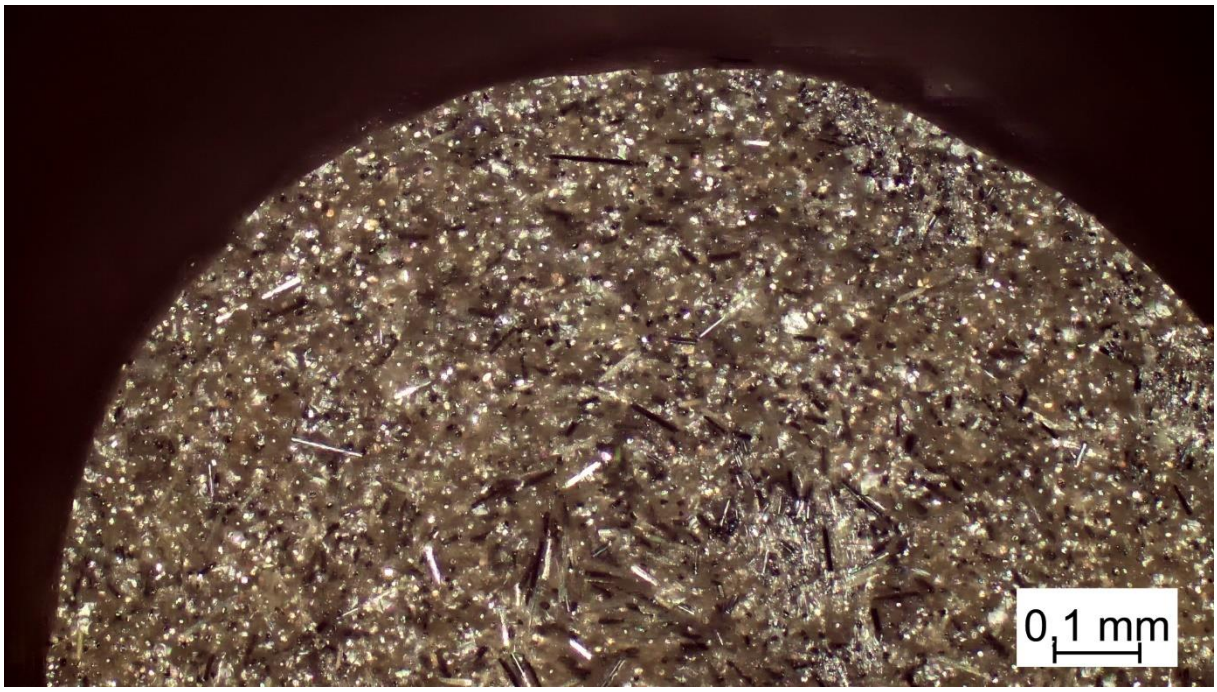

Figure 16: Microscopy of CPC_CF_10 vol.%

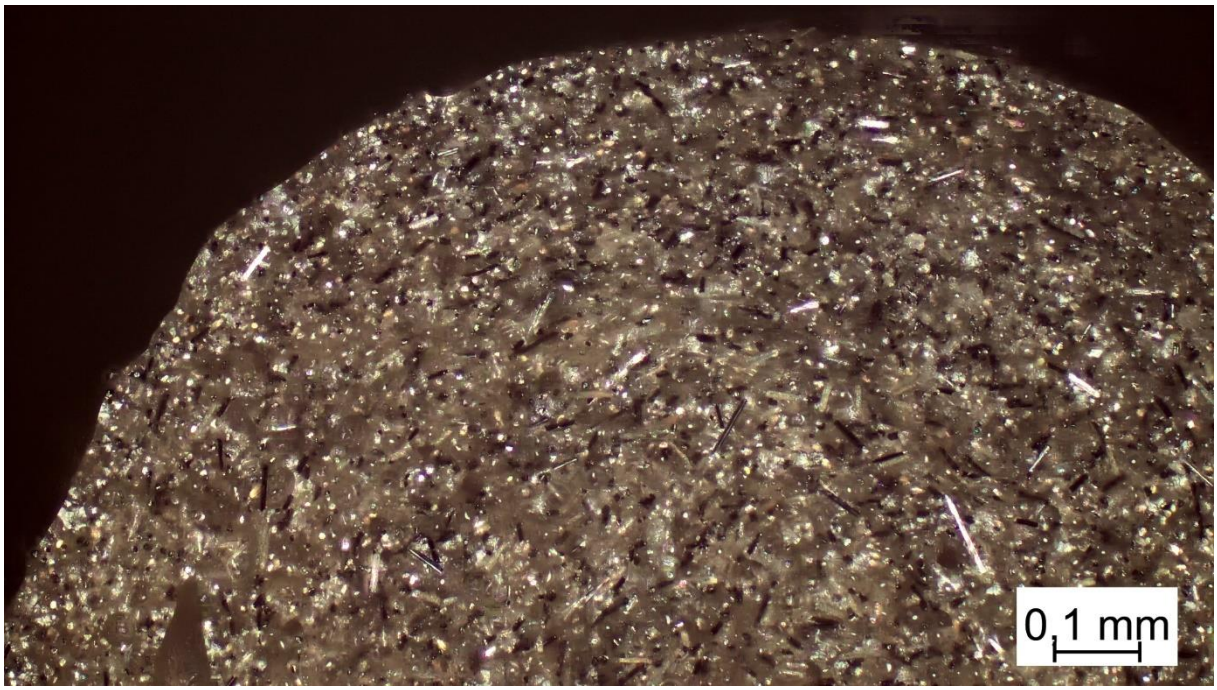

Figure 17: Microscopy of CPC_CF_12.5 vol.%

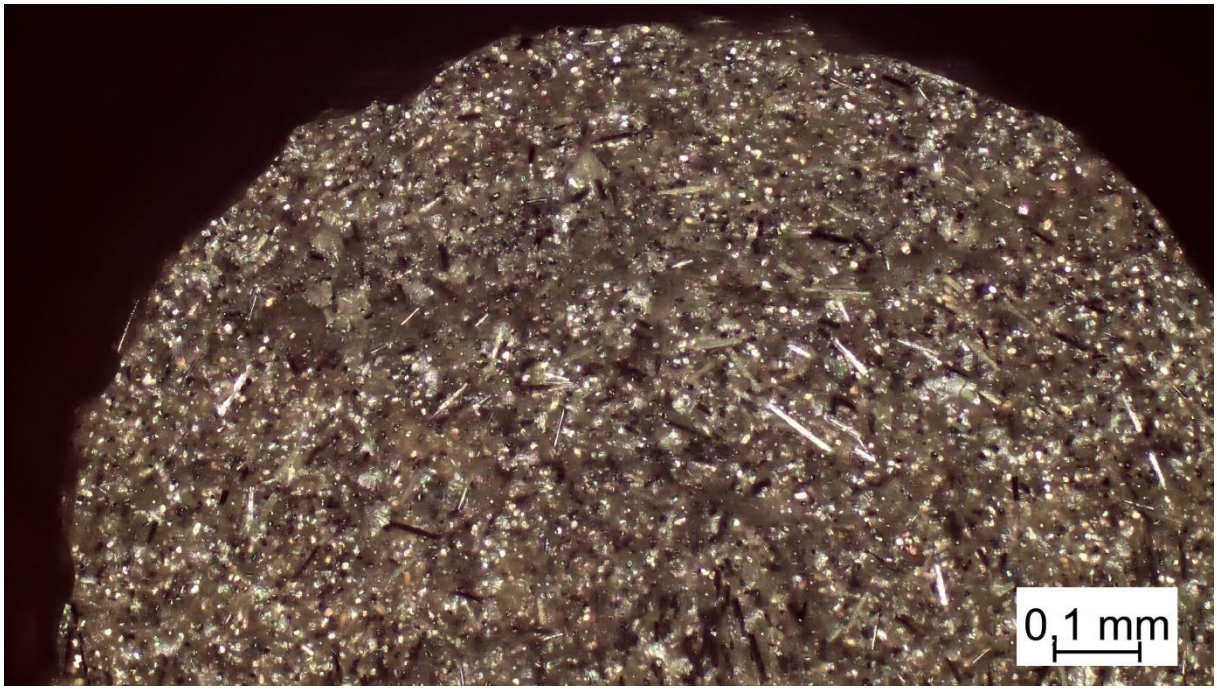

Figure 18: Microscopy of CPC_CF_15 vol.%

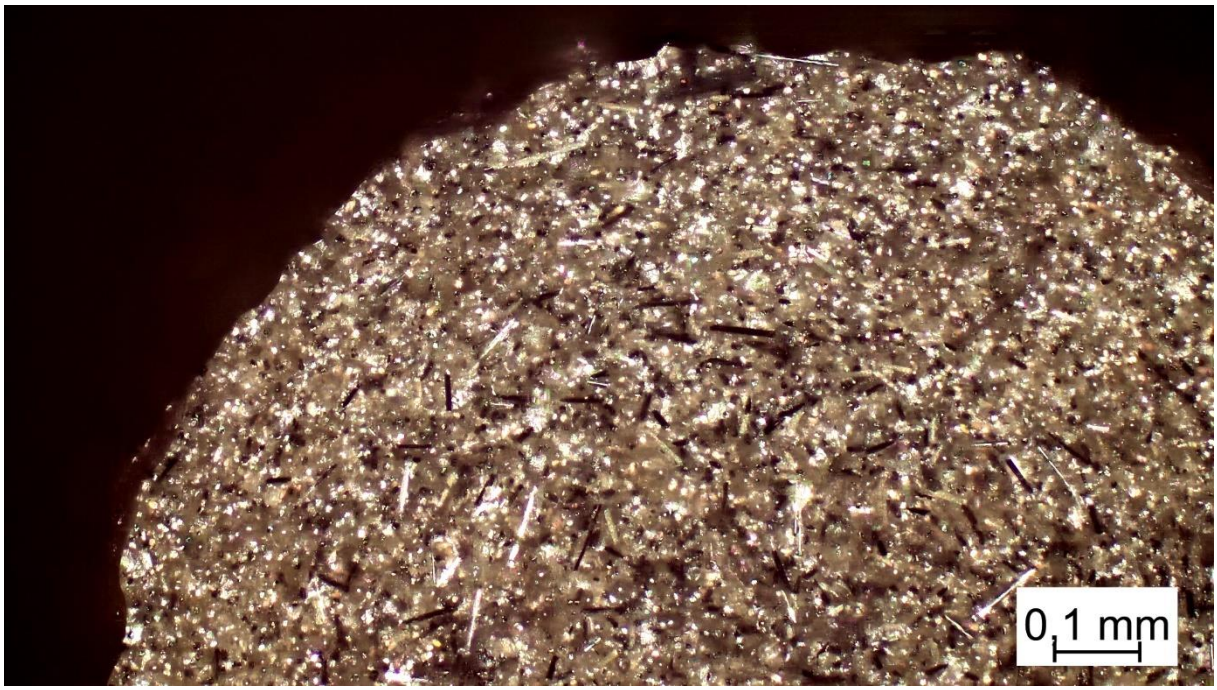

Figure 19: Microscopy of CPC_CF_17.5 vol.%

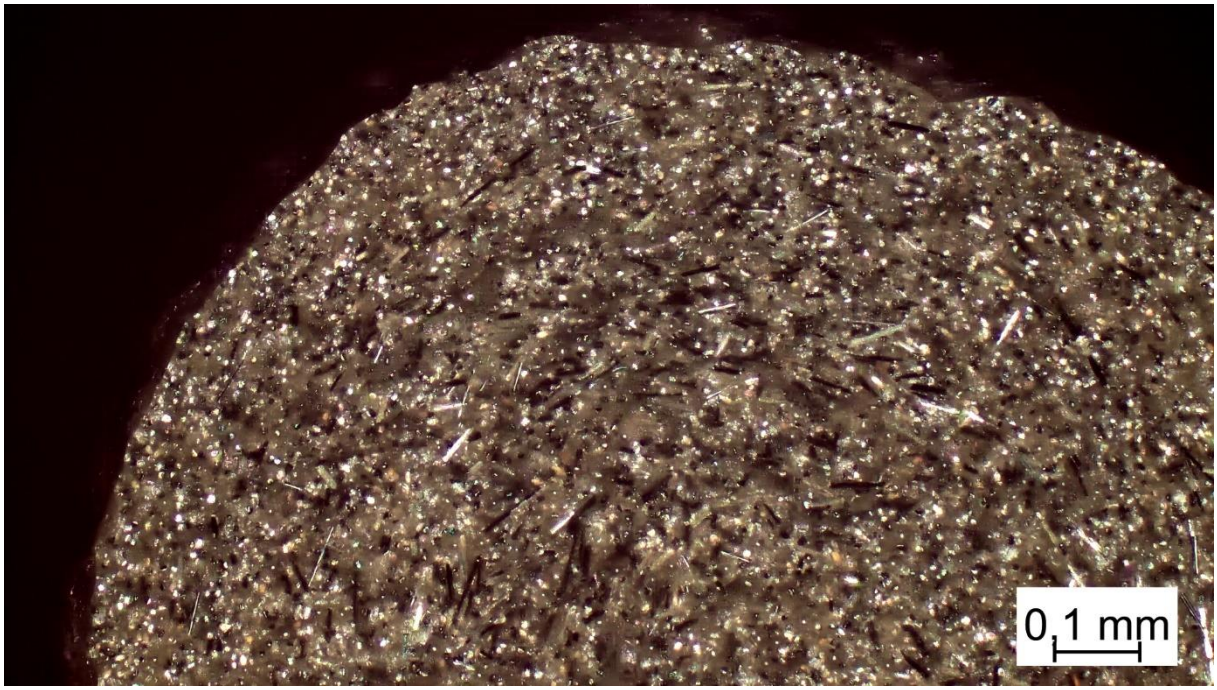

Figure 20: Microscopy of CPC_CF_20 vol.%

From Figure 21 to Figure 24 the CPCs are shown under the light microscope with a filler content of 15 vol.% silver coated carbon fibres and 2.5 and 5.0 vol.% of the two different silver coated glass spheres. The CPC_CF_15-vol.%_GS_5/25_5.0-vol.% showed a void in the filament (Figure 24). Again, the fillers are well dispersed and the polarization filter was set to 0 °, which was again the reason for some particles to appear black.

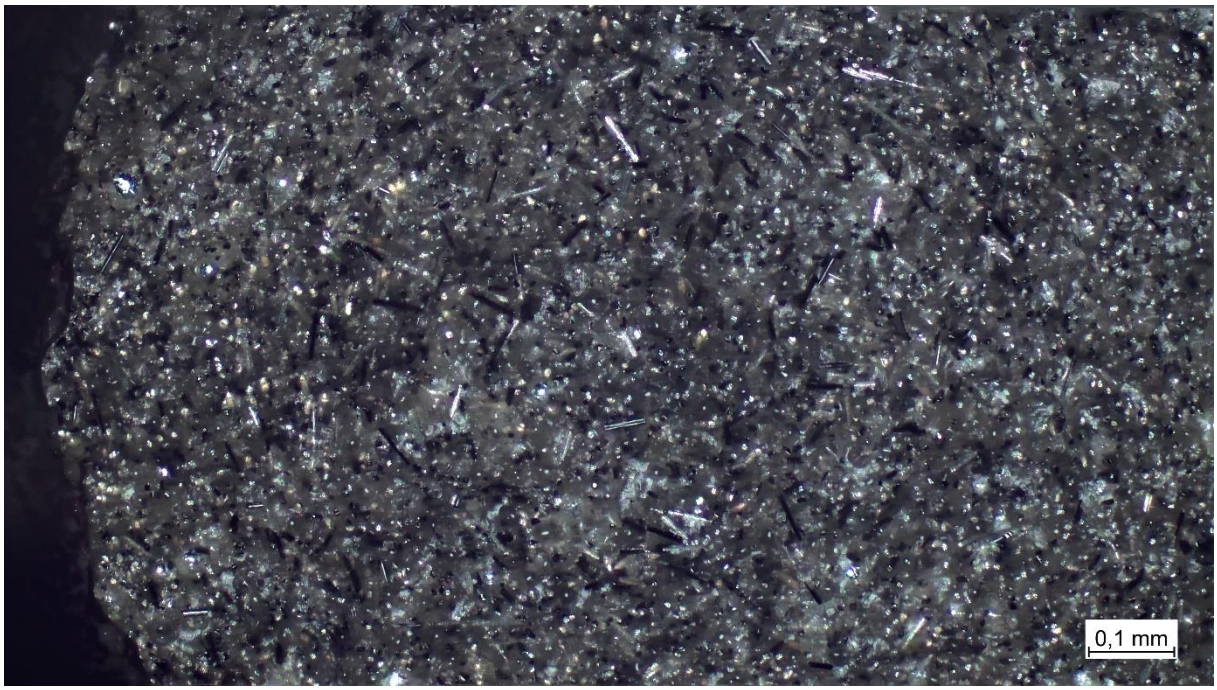

Figure 21: Microscopy of CPC_CF_15-vol.%_GS_35/8_2.5-vol.%

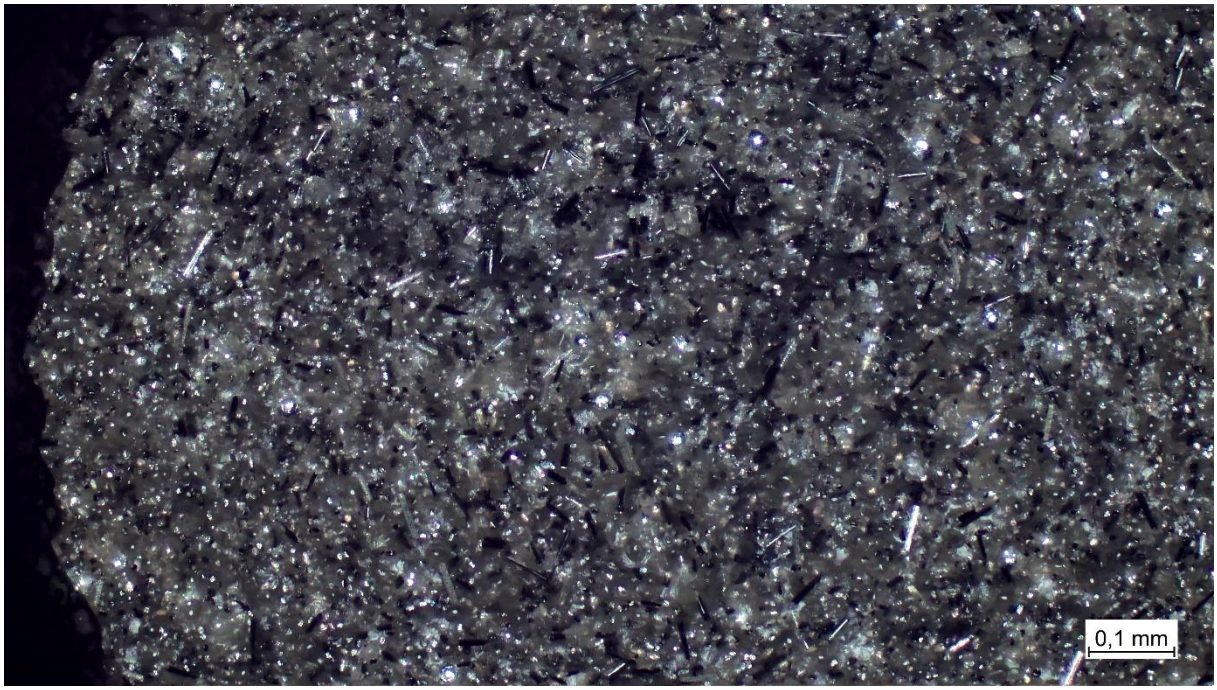

Figure 22: Microscopy of CPC_CF_15-vol.%_GS_35/8_5.0-vol.%

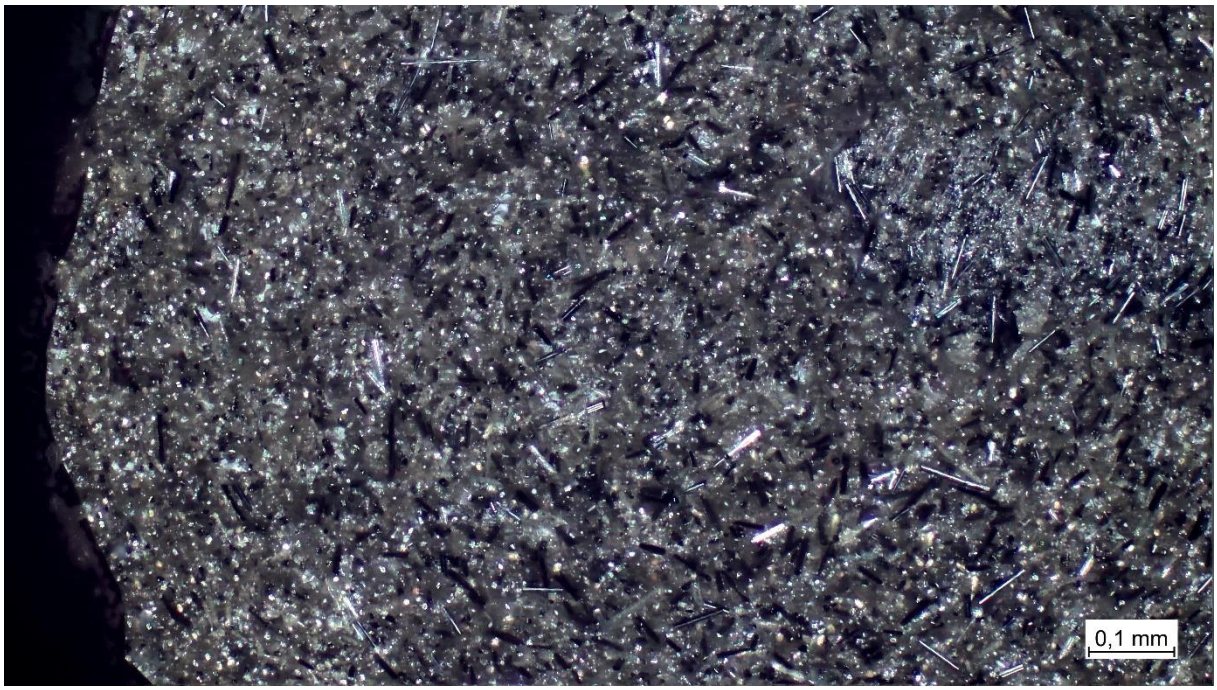

Figure 23: Microscopy of CPC_CF_15-vol.%_GS_5/25_2.5-vol.%

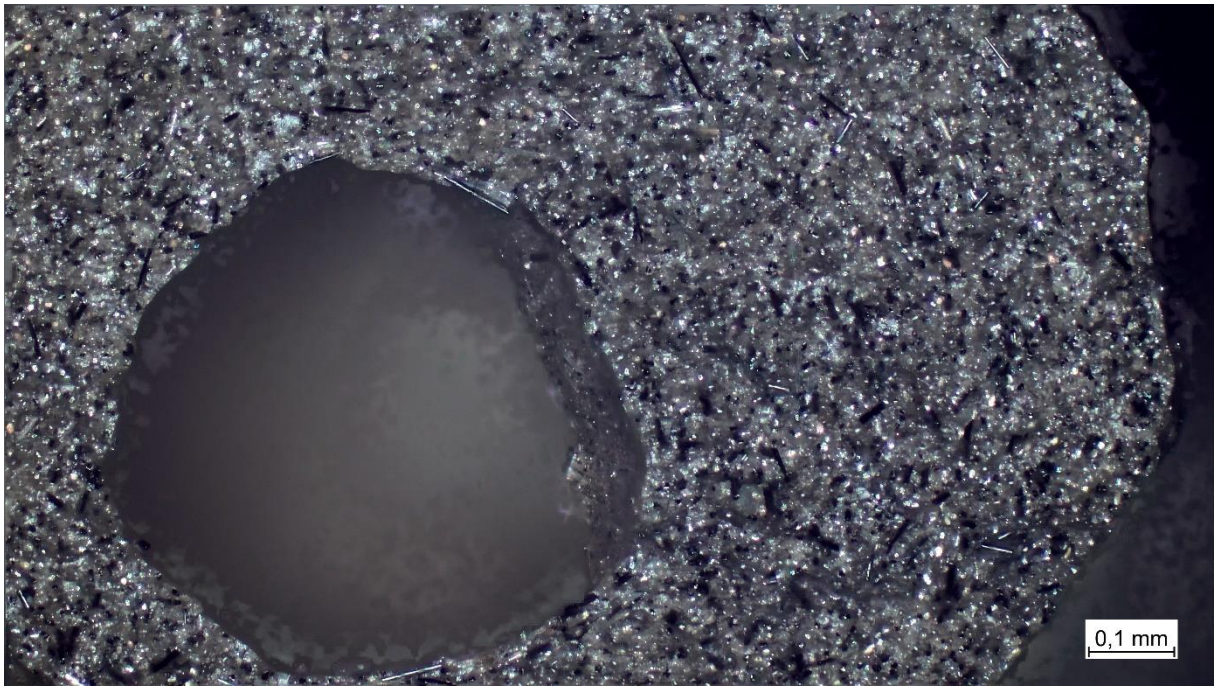

Figure 24: Microscopy of CPC_CF_15-vol.%_GS_5/25_5.0-vol.%

4.3.2 Scanning Electron Beam Microscopy

In all scanning electron beam microscopy figures the settings are in a) backscattered elctones (BSE) and in b) secondary electrons (SE) and the magnification is 500 times.

From Figure 25 to Figure 29 the CPCs are shown under the scanning electron beam microscope filled with just silver coated carbon fibres, reaching from 10 vol.% to 20 vol.% by steps of 2.5 vol%. The scanning electron beam microscope was used supportive for a higher resolution of the matrix and particles. In those pictures the pull-out holes of the fibres can be seen on the fracture surface.

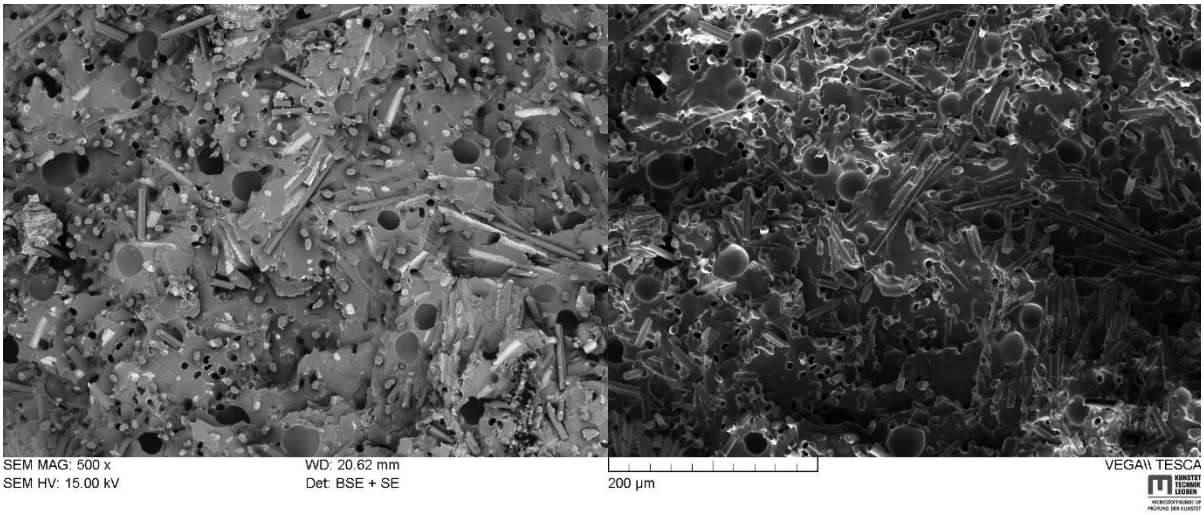

(a) (b)

Figure 25: SEM of CPC_CF_10 vol.%

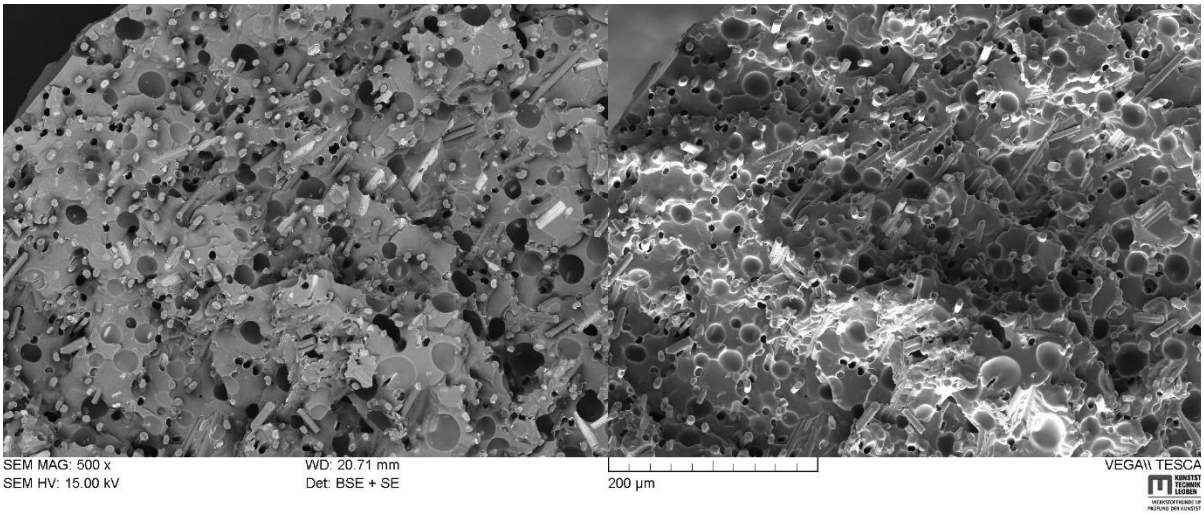

(a) (b)

Figure 26: SEM of CPC_CF_12.5 vol.%

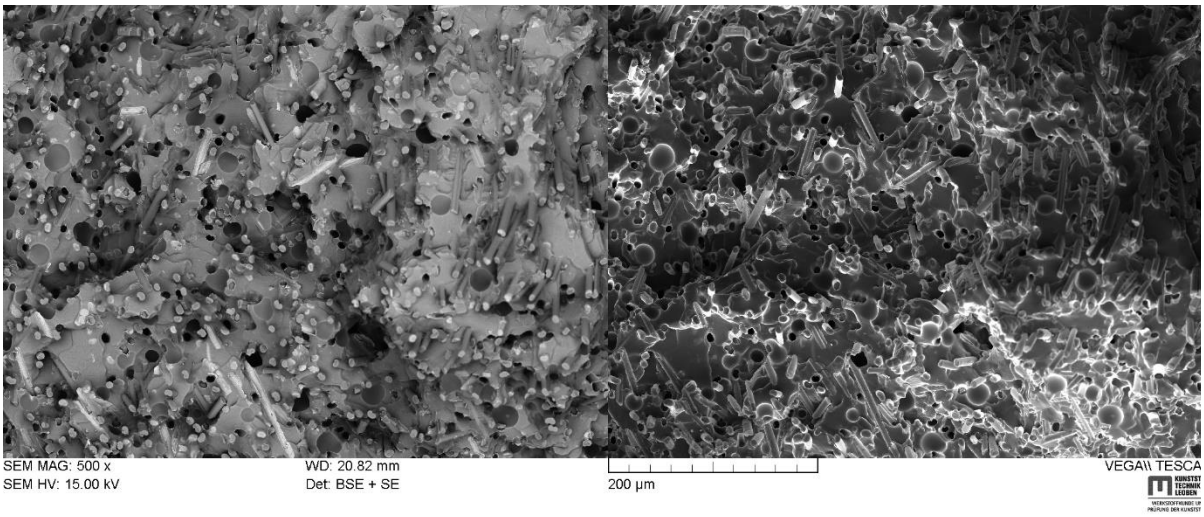

(a) (b)

Figure 27: SEM of CPC_CF_15 vol.%

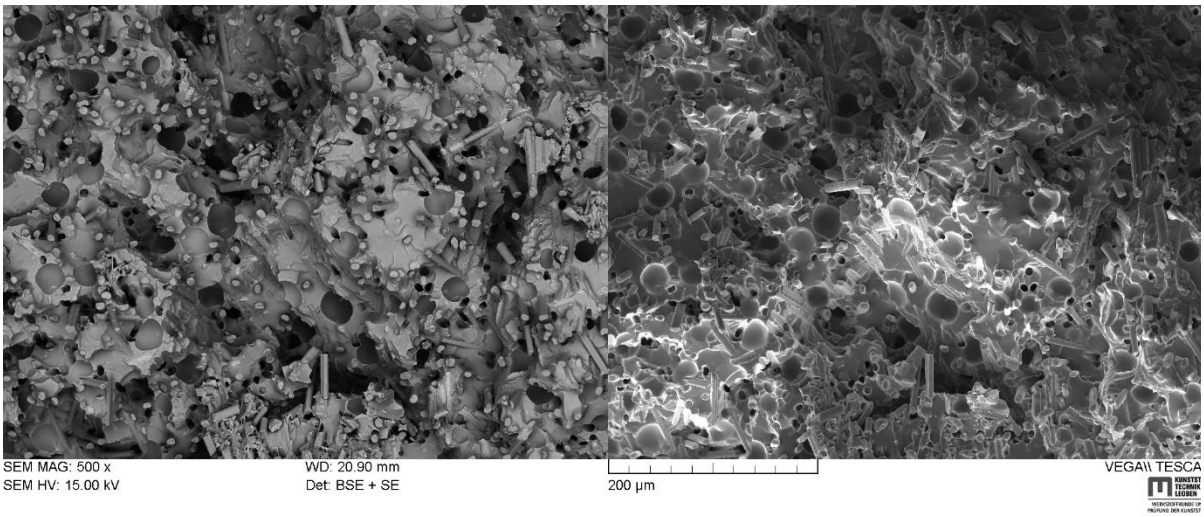

(a) (b)

Figure 28: SEM of CPC_CF_17.5 vol.%

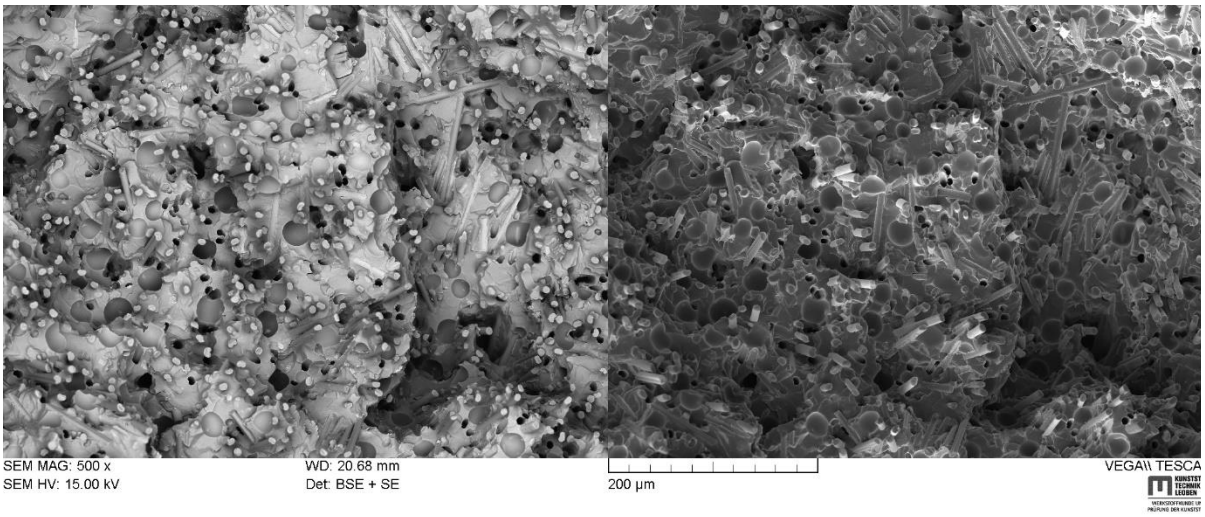

(a) (b)

Figure 29: SEM of CPC_CF_20 vol.%

From Figure 30 to Figure 33 the CPCs are shown under the scanning electron beam microscope with a filler content of 15 vol.% silver coated carbon fibres and 2.5 and 5 vol.% of the two different silver coated glass spheres. What else can be seen is that there cannot be seen any spheres in the area of fraction, because they do not incorporate with the matrix and leaving only the holes.

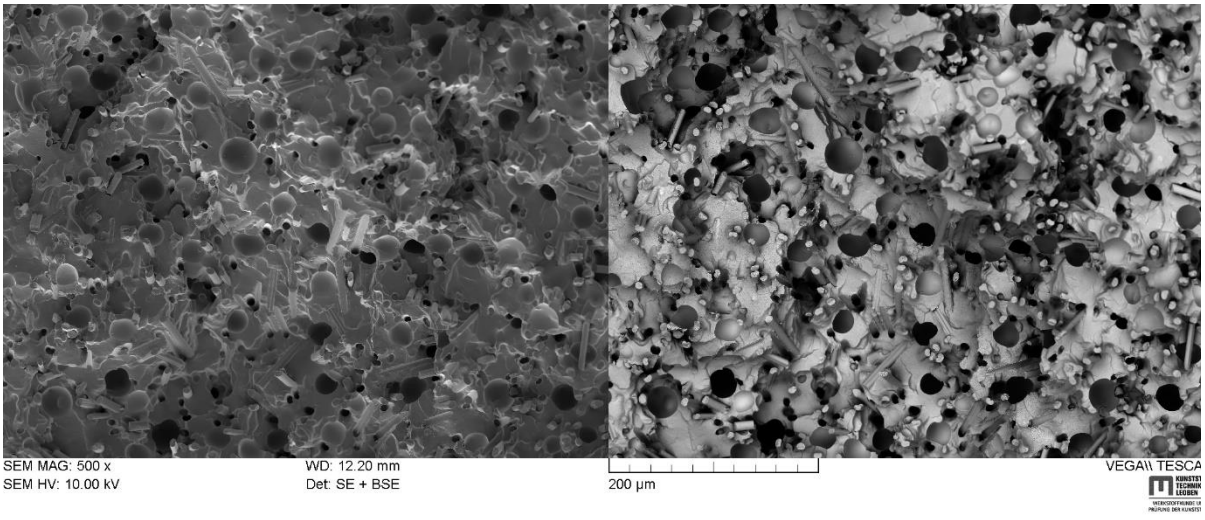

(a) (b)

Figure 30: SEM of CPC_CF_15-vol.%_GS_35/8_2.5-vol.%

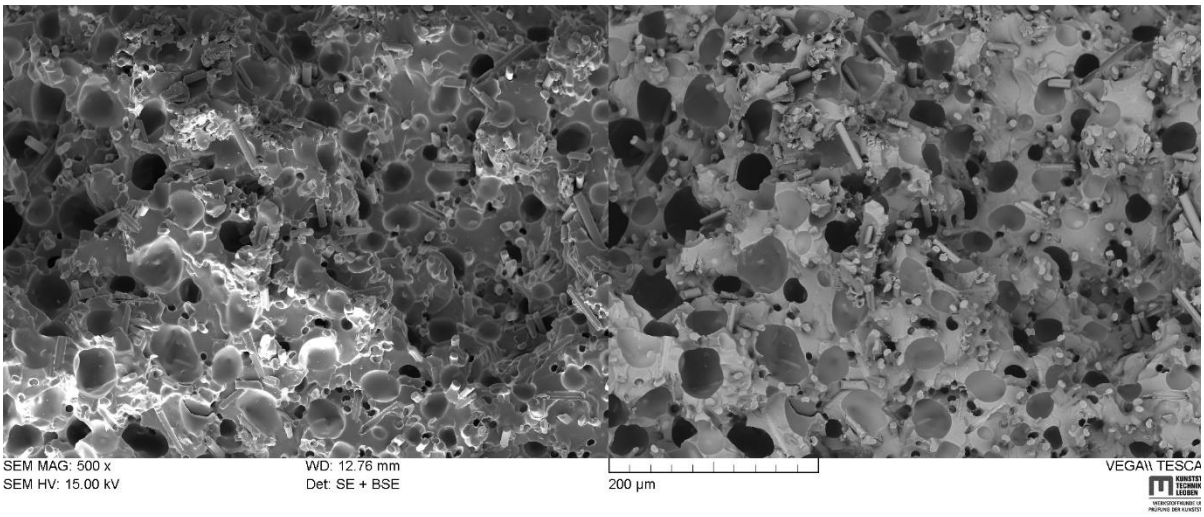

(a) (b)

Figure 31: SEM of CPC_CF_15-vol.%_GS_35/8_5.0-vol.%

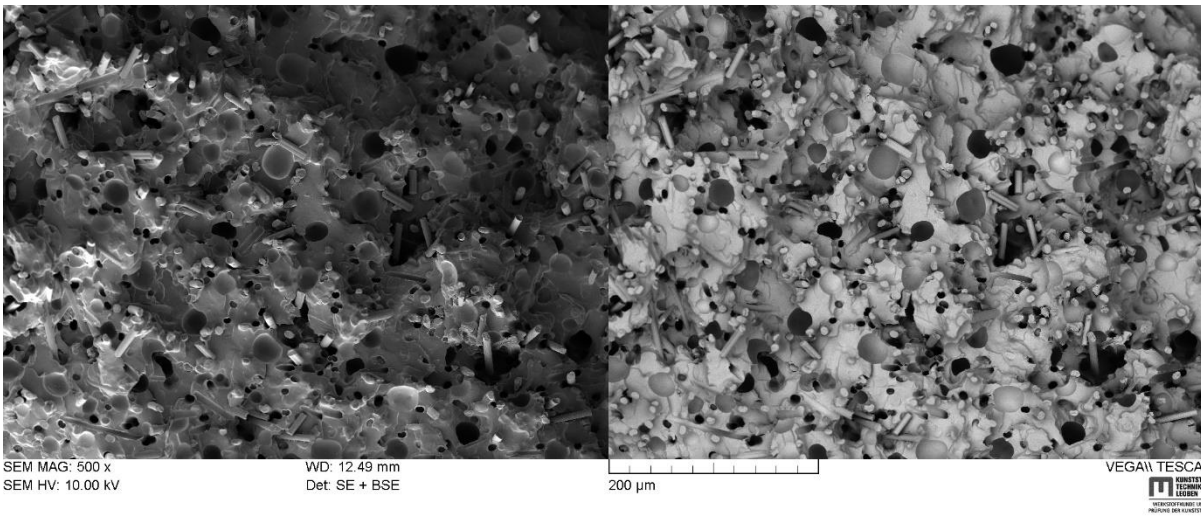

(a) (b)

Figure 32: SEM of CPC_CF_15-vol.%_GS_5/25_2.5-vol.%

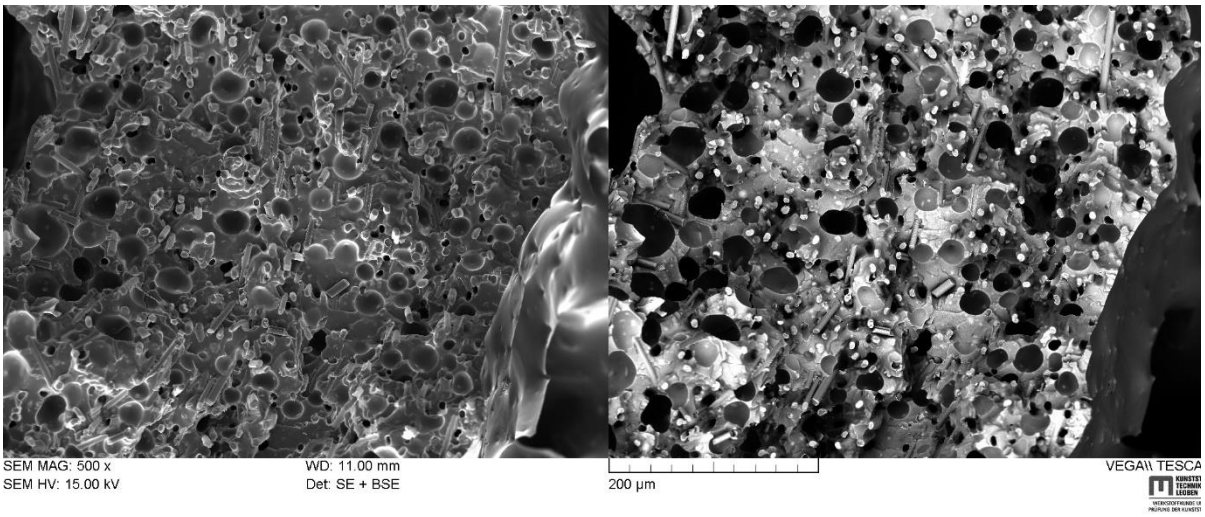

(a) (b)

Figure 33: SEM of CPC_CF_15-vol.%_GS_5/25_5.0-vol.%

4.4 Tensile Tests

In Figure 34 the tensile tests are shown from the CPCs only filled with silver coated carbon fibres. A reference curve of each CPC formulation is plotted with the mean value and standard deviation. The Young's moduli of all tensile tests are presented in Figure 35 along with their mean values and standard deviations. Figure 36 shows additional the mean values of the elongation at break again with their standard deviations. Three repetitions were made for each CPC and maximum one outlier was omitted.

A higher Young's modulus is achieved with a higher carbon fibres content, as shown in Figure 35. This is because of the increased interactions of the fibres with the matrix. It needs more energy for not just matrix failure, but also debonding of the fibres and the matrix, or pull-outs of the fibres. Thus, the filament's modulus and its stiffness increases, because of the need for a higher amount of energy to break the filament [33]. A reduction in elongation at break of the filaments is also caused by the increased stiffness (Figure 36). As well as the elongation at break, also the breaking stress can be seen in Figure 34, where an increase by the rising carbon fibre content can be detected.

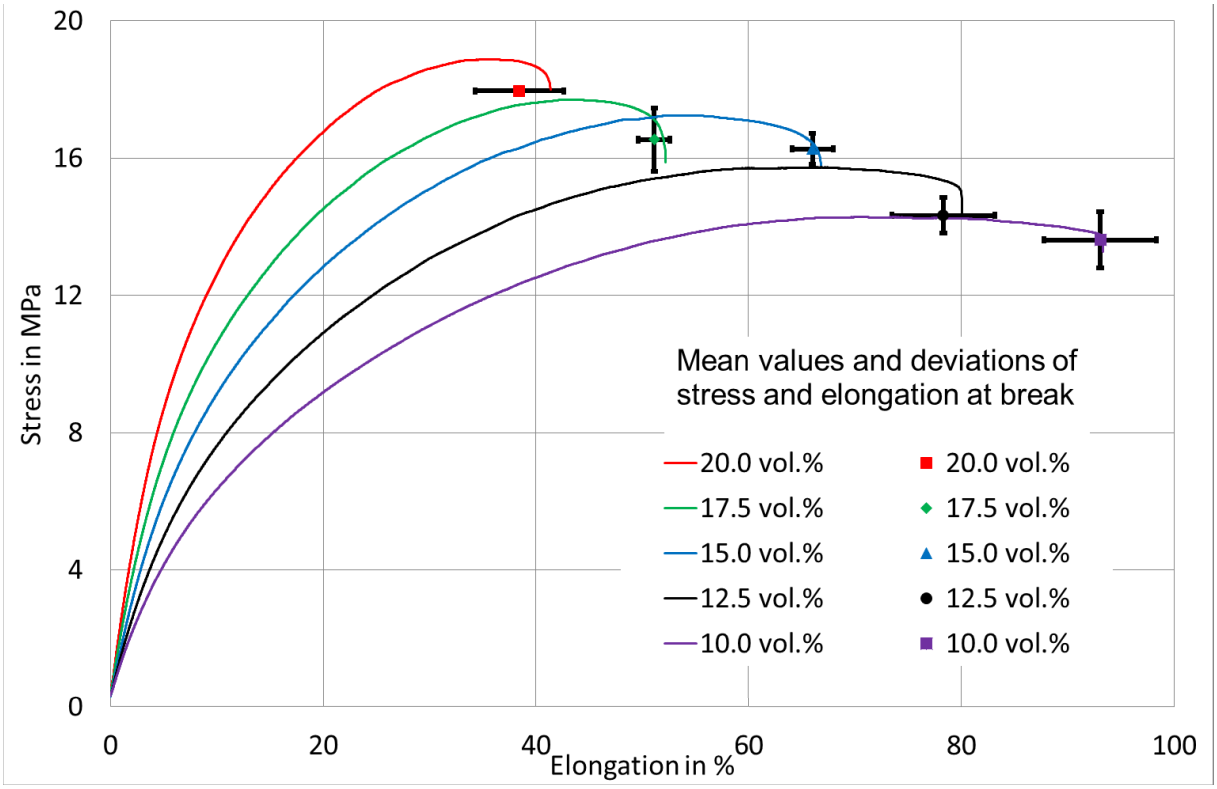

Figure 34: Tensile tests of all CPCs filled with carbon fibres and their mean values and deviations stress and elongation at break

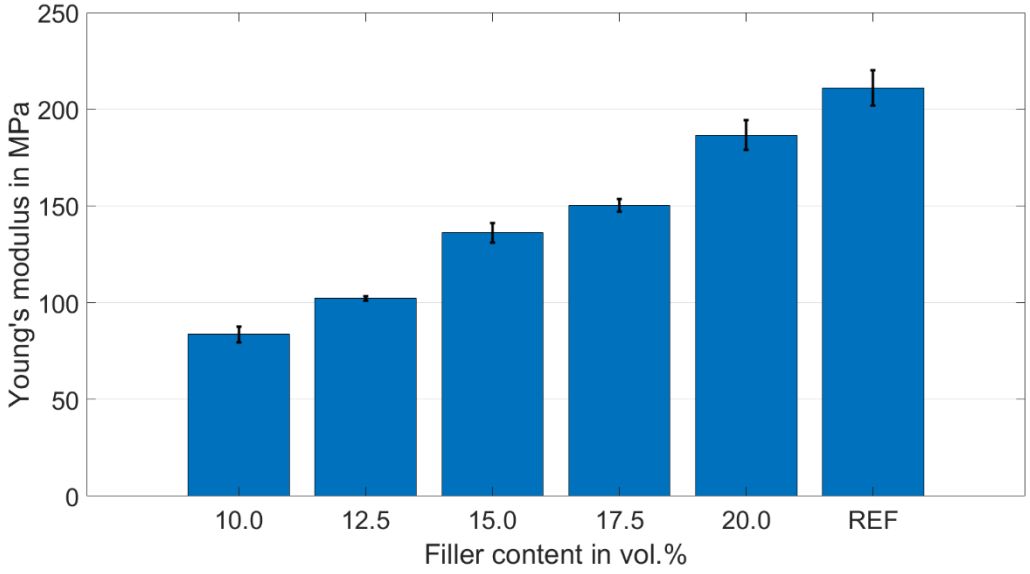

Figure 35: Influence on the Young's modulus by filler content compared to the reference material for CPCs only filled with silver coated carbon fibres

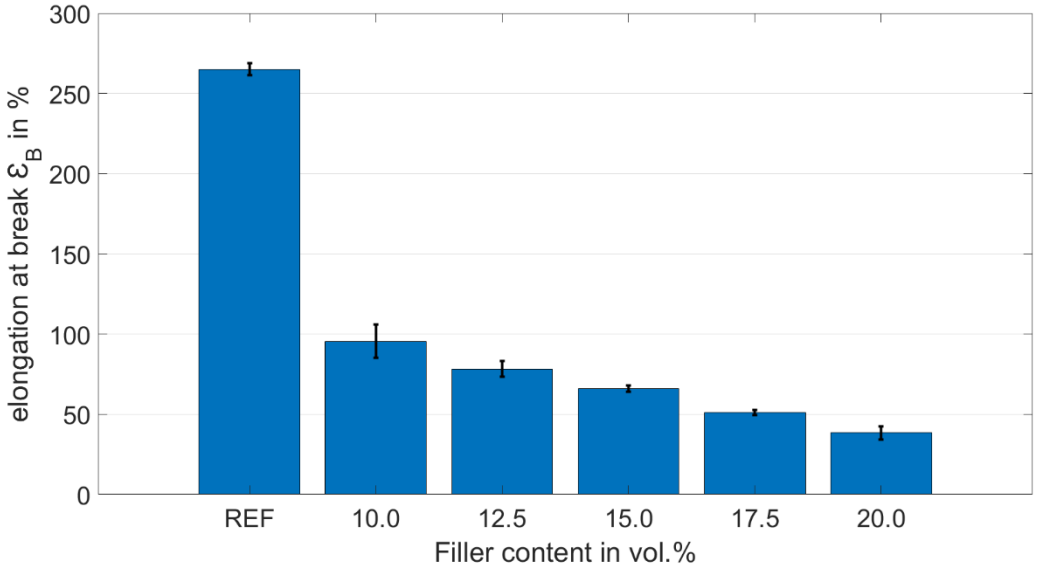

Figure 36: Influence on the elongation at break by filler content compared to the reference material for CPCs only filled with silver coated carbon fibres

The tensile tests of the CPCs filled with 15 vol.% carbon fibres and the different spheres are shown in Figure 37. In Figure 38 again all Young's moduli of the CPCs with carbon fibres and spheres are listed. Figure 39 illustrates the influence of the fillers on the elongation at break with their mean values and also standard deviations. Additionally, the CPC_CF_15-vol.% is shown for comparison in all three prementioned figures.

Compared to the filaments only filled with carbon fibres, the spheres lead to a decrease of the Young's modulus (Figure 38). The reason for that is the decrease in cross sectional area of load bearing matrix and that stress concentrations at the sphere's regions occur. This effect is also found in the literature [22]. The elongation at break also decreases by using bigger spheres. The spheres can be seen as inhomogeneities and lead to an early breaking of the filament. The bigger the sphere, the bigger the inhomogeneity and the higher the probability of failure [35].

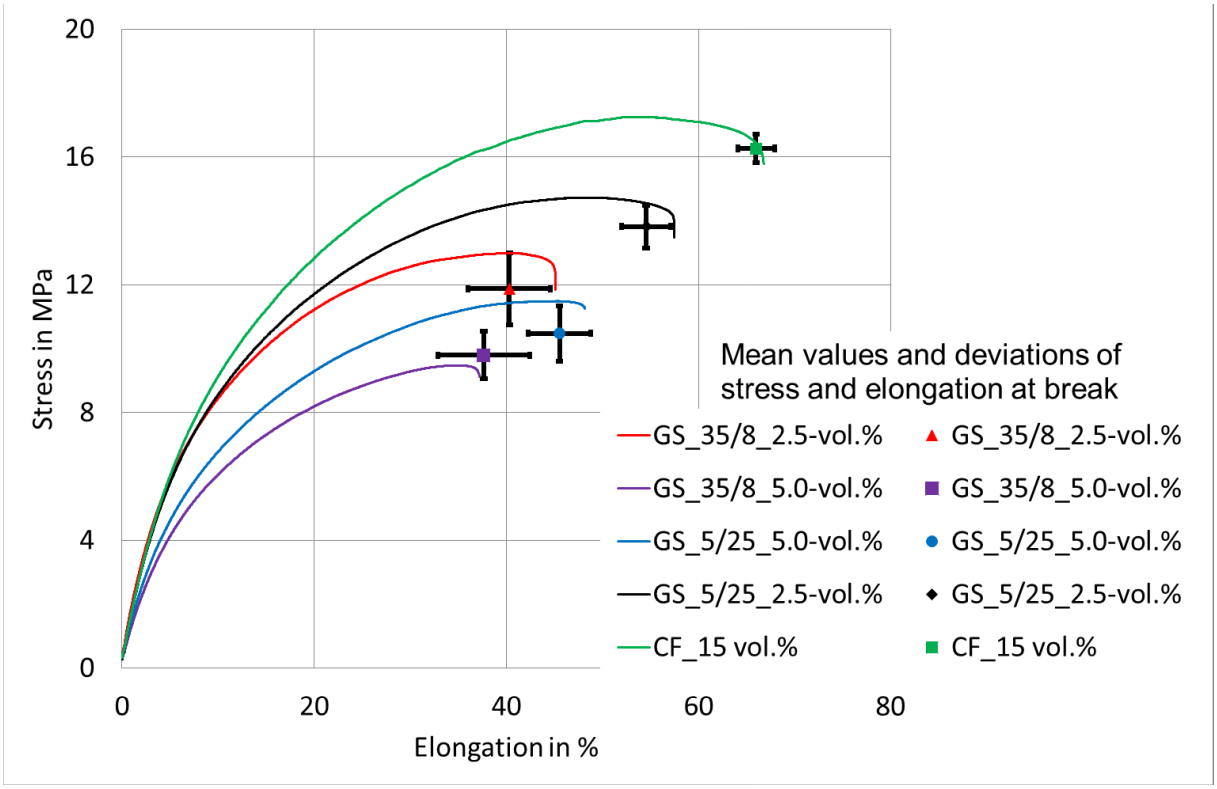

Figure 37: Tensile tests of all CPCs filled with 15 vol.% carbon fibres and two different kind of glass spheres

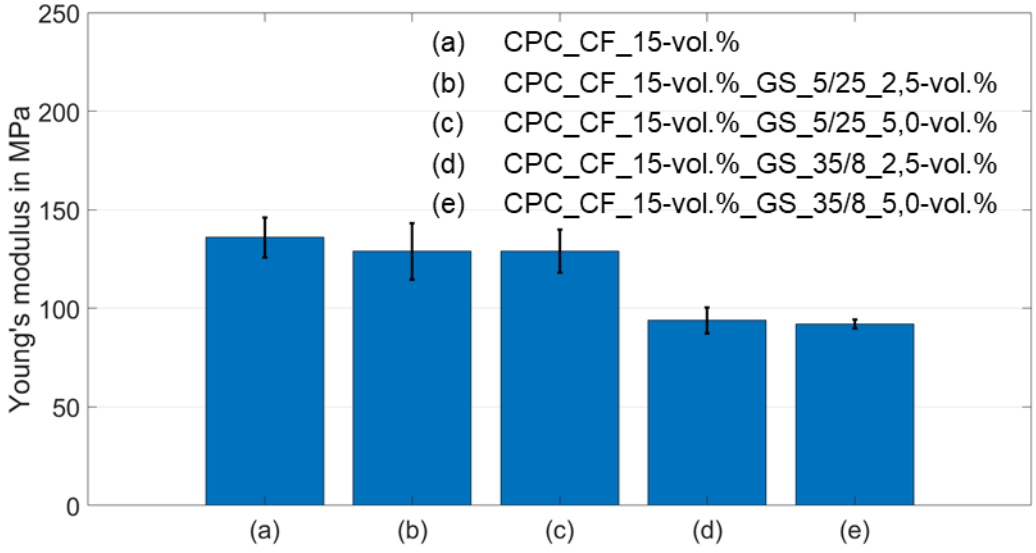

Figure 38: Influence on the Young's modulus by filler content for CPCs filled with 15 vol.% silver coated carbon fibres and spheres

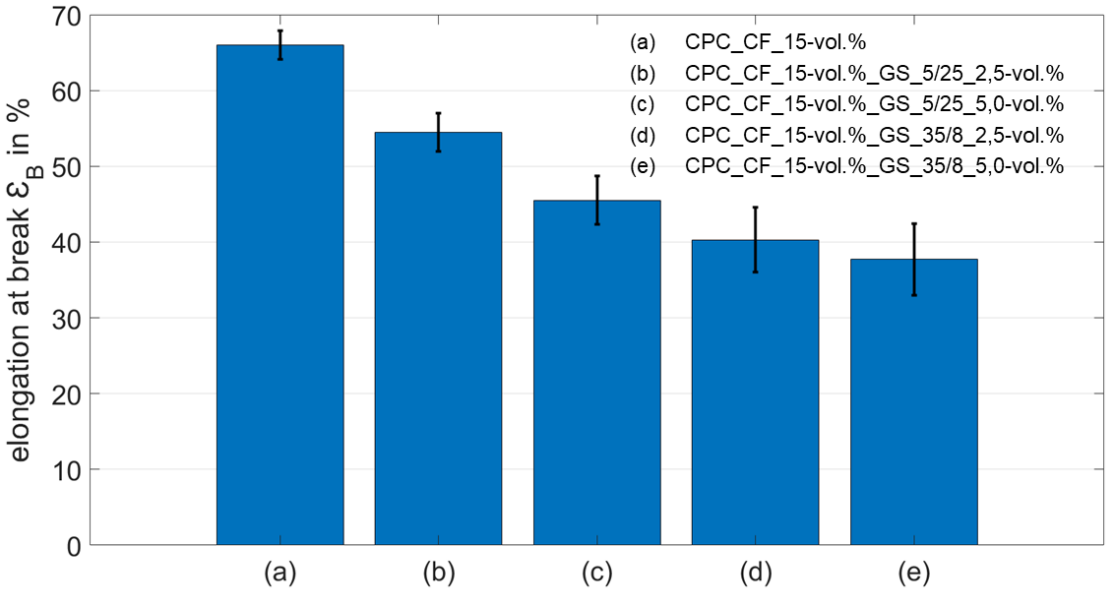

Figure 39: Influence on the elongation at break by filler content for CPCs filled with 15 vol.% silver coated carbon fibres and spheres

4.5 Electrical Resistance

In Figure 40 the measured resistances of the CPCs filled with carbon fibres are shown. For each filament, three repetitions were made. For comparison the reference material (a) is also listed in this graph. In Figure 41 are the CPCs, which are again filled with 15 vol.% carbon fibres and glass spheres.

For the CPC_CF_10-vol.% there was no electric conduction ascertainable, even at high voltages. For the CPC_CF_12.5-vol.% there was the first electric conduction measurable with a resistance of 2.45 ± 0.24 kΩ/cm. The CPCs with 15 to 20 vol.% led to even better conductivity in the range of 0.63 – 0.77 kΩ/cm (Figure 40).

Anyhow, what has to be said is that an impulse of 2 kV was needed to achieve electric conduction for the aforementioned filaments. In the literature it was found that due to the high voltages the particles, besides getting charged, also heat up, which leads to a breakdown and burning of the insulative matrix around the fillers which leaves a conductive carbon path. The electron transport in CPCs is well described in [29]. In Figure 44 there is an exaggerated example of the carbon path visible, where the CPCs were used for heating applications. The voltage was indeed lower (< 1 kV) but held for a long time until it came to the burning of the material.

For the CPC_CF_15-vol.%_GS_5/25_5.0-vol.% there was no impulse needed. The small spheres were enough to increase the contact between the fibres and allow electric conduction at lower voltages. Moreover, the best conduction was achieved with this filament with a resistance of 0.21 ± 0.07 kΩ/cm (Figure 41). It has to be said that the resistance continuously decreased by increasing the voltage. At a voltage of around 1 kV the resistance stayed the same. Corresponding to literature it was found that there are two ways of electric conduction. The first is the conduction due to a conductive path and the second is caused by strong electric

fields. The spheres in the CPC increased the contacts between conductive fillers, but the dominant electron transport mechanism was electron tunnelling. According to theory there is a strong dependence on the resistance to the voltage. The decrease of the resistance by the increase of voltage is also found in the literature. The decrease is because of the fact that there is a change of two transport mechanisms of electron tunnelling. Those are trap-induced and trap-free space charge limited current (SCLC). In the transport mechanism of trap-induced SCLC not all electrons in the valenz-bond take part in the transport mechanism and they are held back in energy traps. At higher voltages those traps vanish and the electrons can move freely in the electric fields and there is the change to trap free SCLC [24, 29]. For the CPC_CF_15-vol.%_GS_5/25_5.0-vol.% it is not clearly to say, if the building up of a carbon path due to burning of the material or the change of trap-induced to trap-free SCLC is the dominant transport mechanism in the CPC.

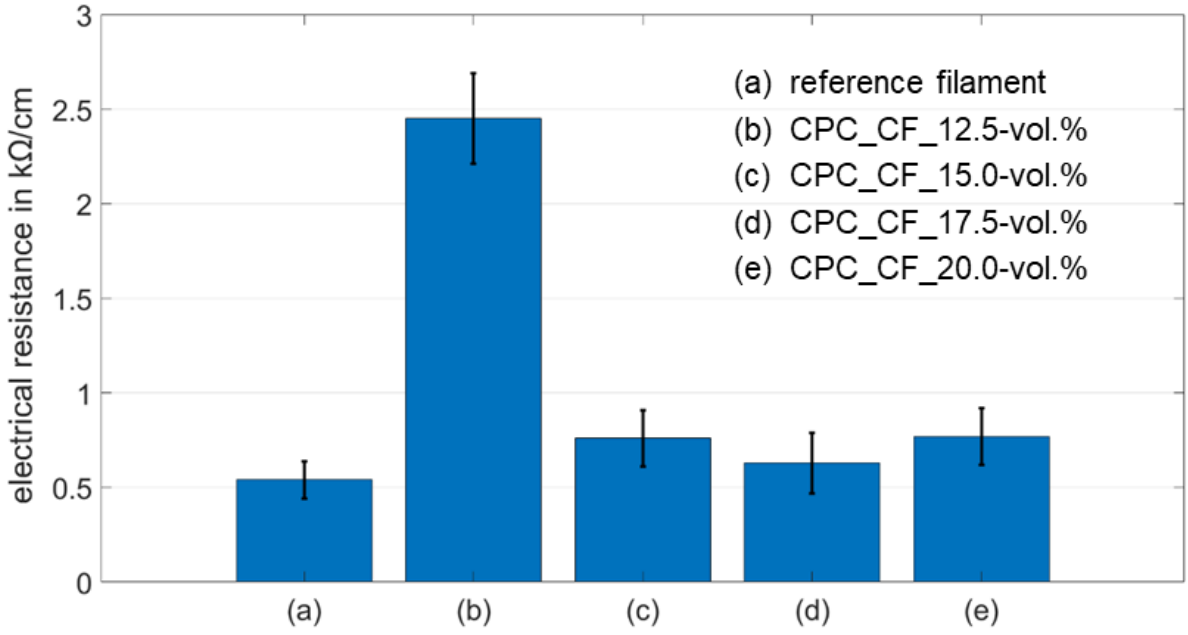

Figure 40: Measurement of electrical resistance from CPCs with silver coated carbon fibres

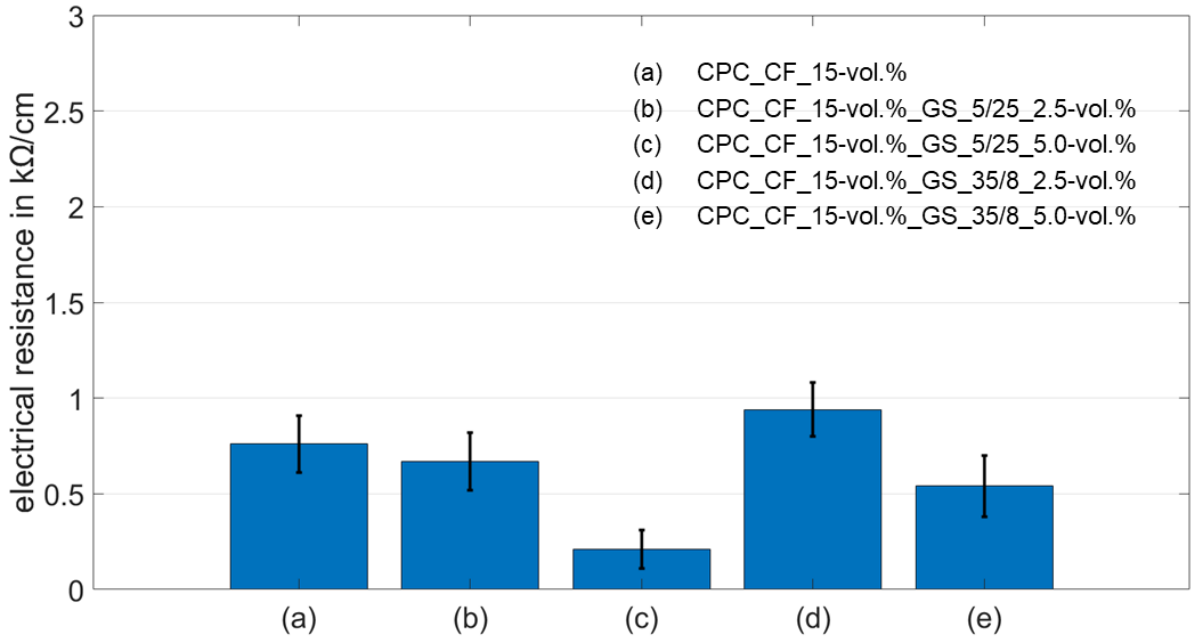

Figure 41: Measurement of electrical resistance from CPCs with 15 vol.% carbon fibres and different amounts and sizes of glass spheres

4.6 Material Extrusion

In Figure 42 the DEA is portrayed with the electrode material CPC_CF_15-vol.% with no applied voltage. In Figure 43 the voltage of 2.8 kV was applied and a displacement of 110 % was achieved. For the CPC_CF_17.5-vol.% the same results were achieved and for the CPC_CF_12.5-vol.% a little movement was observed but not measurable. For the CPC_CF_20-vol.% and the CPCs filled with 15 vol.% carbon fibres and spheres the filament was not extrudable and DEAs were not able to be printed. For heating applications, the CPC_CF_15-vol.% was tried to be printed as heating elements, displayed in Figure 44.

For the printed DEA the best result was achieved with the CPC_CF_15-vol.%, as well as with the CPC_CF_17.5-vol.% the same results were reached. However, CPC_CF_20-vol.% was not printable due to some troubles that occurred. Then it was tried to use the CPC material for heating application, but due to poor contacts between the fillers it came to local hot spots, which led to burning of the material. The heating trials are visible in Figure 44.

To improve the conductivity and allow to use the CPCs for heating applications, the conductive behaviour and contacts between the fibres were improved by adding glass spheres. The bigger spheres with a D50 value of 35 µm had no influence on the conductivity but the smaller spheres with a D50 value of 5 µm turned out to reduce the resistance to 0.21 ± 0.07 kΩ/cm. Also, no impact of 2 kV was needed, which made it quite promising for heating applications.

Anyhow, the troubles with the CPC_CF_20-vol.% remained true for the CPCs filled with 15 vol.% carbon fibres and glass spheres. The main problem of those CPCs was the improved thermal conductivity of the filaments. This led to a too early softening of the material, which means that

it wasn't extrudable anymore. The filament got spiralled between the extruder and the heating element and was not pushed through the nozzle. For the CPC_CF_12.5-vol.% a little but not measurable movement was visible, which means that the electric field built-up was not strong enough to allow the DEA to bend.

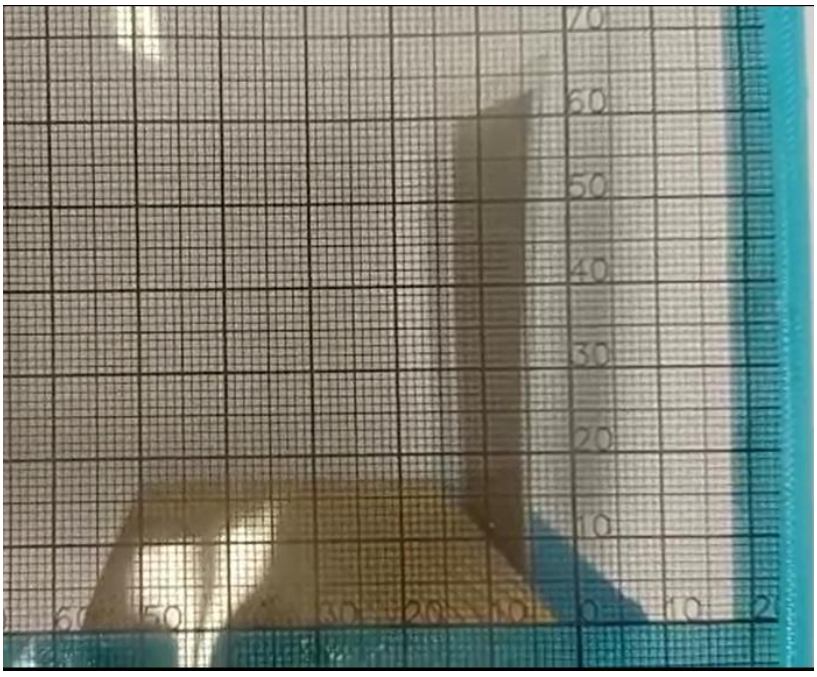

Figure 42: Dielectric Elastomer Actuator (electrode material: CPC_CF_15-vol.%) with no applied voltage

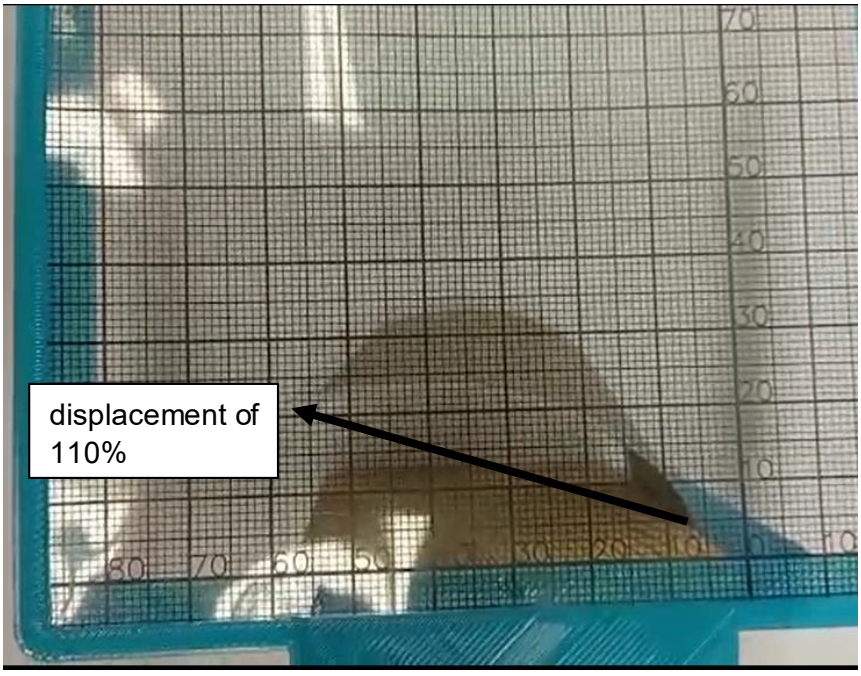

Figure 43: Dielectric Elastomer Actuator (electrode material: CPC_CF_15-vol.%) with 2.8 kV

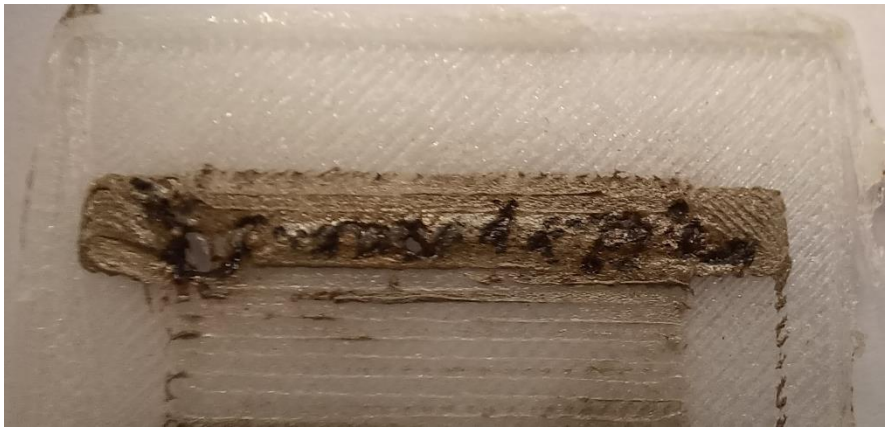

Figure 44: Burnt material for heating applications at lower voltages (< 1 kV) with CPC_CF_15-vol.%

5 Conclusion and Outlook

Aim of this work was to improve the electrodes of Dielectric Elastomer Actuators. By setting up different formulations with a specific TPE type as matrix and different filler types, which were silver coated, it turned out that the silver coated carbon fibres behaved the best for this application. After the first kneading trials and filament extrusions, the first actuators were printed. For the CPC_CF_15-vol.% it emerged, that the DEA already achieved the same displacement as the reference with half of the applied voltage. Therefore, on step further was planned to use the CPC filaments for heating applications. For the CPC_CF_15-vol.% an intrinsic heating was printed and a voltage < 1 kV was applied. Due to the poor contacts between the carbon fibres in the CPC it came to local overheating of the fillers and burning of the material. That is why silver coated glass spheres of two different sizes have been added to the carbon fibres to improve the interfibre contacts. When measuring the resistance of the new formulations with carbon fibres and glass spheres it was found that the smaller spheres were more effective at decreasing the resistance of the CPC. In addition, it should be noted that for all the CPC an impact of 2 kV was needed to achieve electric conduction. Anyhow, not for the CPC_CF_15-vol.%_GS_5/25_5.0-vol.%, where a decrease of the resistance by the increase of the voltage was ascertainable. With this CPC the printing of heating applications has been attempted again. As a consequence of the high infill of silver coated fillers, CPCs also showed improved thermal conductivity. The filament softened too early in the printer, so it was no longer extrudable and spiralled.

It appears, however, that the in advance set goals of improving electrodes have been achieved, as there was just about half the voltage needed to maintain the same displacement as the reference electrodes. Nevertheless, for heating applications the electrodes failed, because the CPCs with higher conductivity were not processable and for the printable filaments the conductivity was not sufficient enough and it came to burning of the material.

To improve the processability of the CPCs and to reduce the thermal conduction further steps have been taken in account. The first one was the replacement of the pure TPE with a conductive TPE (TPE + specific carbon structure) to reduce the thermal conductivity. Due to the conductive matrix less amount of silver coated fillers was expected to achieve electric conductivity. Despite this, the matrix was too soft, and the filament was rubbed off in the extruder as a result. In an attempt to reduce filament abrasion, conductive TPE was mixed with pure TPE, but it failed again to be printed.

It is also possible to prevent thermal problems by using nozzles with better cooling systems or different conveying methods in the printer which are not that affected, if the filament softens before it reaches the nozzle.

Furthermore, the filaments were made on a capillary rheometer where the diameter of the filament could only be adjusted by manually setting the speed of the conveyer belt. Due to this, a diameter fluctuation can be expected and should be taken into account during printing. Those fluctuations led to voids in the DEA and behave as insulator between the conductive particles.

Summing up it can be said that this field of DEAs has a lot of potential in research and development and there is still a lot to do, to find conductive enough CPCs in form of filaments for such applications. In search of implementations, DEAs show their potential in soft robotics acting as soft grippers for light weight and sensitive parts.

6 Literature

[1] Bandyopadhyay, A.; Bose, S.: Additive Manufacturing, Second Edition, 2. Ed., CRC Press LLC, Milton, 2019

[2] Brochu, P.; Pei, Q.: Advances in dielectric elastomers for actuators and artificial muscles, Macromolecular rapid communications 31 (1), 2010, pp. 10–36

[3] Brochu, P.; Pei, Q.: Dielectric Elastomers for Actuators and Artificial Muscles, In: Rasmussen L. (Hrsg.): Electroactivity in Polymeric Materials, Springer US, Boston, MA, 2012, pp. 1–56

[4] DIN EN ISO 527-2:2012-06, Kunststoffe_- Bestimmung der Zugeigenschaften_- Teil_2: Prüfbedingungen für Form- und Extrusionsmassen (ISO_527-2:2012); Deutsche Fassung EN_ISO_527-2:2012

[5] DIN EN ISO/ASTM 52900:2022-03, Additive Fertigung_- Grundlagen_- Terminologie (ISO/ASTM 52900:2021); Deutsche Fassung EN_ISO/ASTM 52900:2021

[6] Duan, L.; D'hooge, D.R.; Spoerk, M.; Cornillie, P.; Cardon, L.: Facile and Low-Cost Route for Sensitive Stretchable Sensors by Controlling Kinetic and Thermodynamic Conductive Network Regulating Strategies, ACS Applied Materials & Interfaces 10 (26), 2018, pp. 22678–22691

[7] Duan, L.; Spoerk, M.; Wieme, T.; Cornillie, P.; Xia, H.; Zhang, J.; Cardon, L.; D'hooge, D.R.: Designing formulation variables of extrusion-based manufacturing of carbon black conductive polymer composites for piezoresistive sensing, Composites Science and Technology 171, 2019, pp. 78–85

[8] EPFL: Ultra-high voltage (7+ kV) power supply for dielectric elastomer actuators, 2022 (Abgerufen am: 25.04.2022)

[9] Frick, A.: Praktische Kunststoffprüfung, Hanser Verlag, München, 2010

[10] Gibson, I.: Additive Manufacturing Technologies, 3D Printing, Rapid Prototyping, and Direct Digital Manufacturing, Springer eBook Collection Engineering, 2. Ed., Springer New York, New York, NY, 2015

[11] Grellmann, W.; Seidler, S.: Kunststoffprüfung, 3. Ed., Hanser, München, 2015

[12] Gu, G.-Y.; Zhu, J.; Zhu, L.-M.; Zhu, X.: A survey on dielectric elastomer actuators for soft robots, Bioinspiration & biomimetics 12 (1), 2017, pp. 11003

[13] Hajiesmaili, E.; Clarke, D.R.: Dielectric elastomer actuators, Journal of Applied Physics 129 (15), 2021, pp. 151102

[14] Hentschel, L.: Internal presentation about ARBURG freeformer at the institute of polymer processing, Leoben, 2021

[15] Holzner, A.: Lecture notes: Elastomertechnologie I, Leoben, 2021

[16] Inkson, B.J.: Scanning electron microscopy (SEM) and transmission electron microscopy (TEM) for materials characterization, In: Materials Characterization Using Nondestructive Evaluation (NDE) Methods, Elsevier, 2016, pp. 17–43

[17] Kaiser, W.: Kunststoffchemie für Ingenieure, Von der Synthese bis zur Anwendung, 3. Ed., Hanser, München, 2011

[18] Kianian, B.: Wohlers Report 2017: 3D Printing and Additive Manufacturing State of the Industry, Annual Worldwide Progress Report: Chapters titles: The Middle East, and other countries, 2017

[19] Kim, J.; Kim, J.W.; Kim, H.C.; Zhai, L.; Ko, H.-U.; Muthoka, R.M.: Review of Soft Actuator Materials, International Journal of Precision Engineering and Manufacturing 20 (12), 2019, pp. 2221–2241

[20] Kornbluh, R.; Pelrine, R.; Pei, Q.; Heydt, R.; Stanford, S.; Oh, S.; Eckerle, J.: Electroelastomers: applications of dielectric elastomer transducers for actuation, generation, and smart structures, In: Vol. 4698, SPIE, 2002, pp. 254–270
[21] Kwok, S.W.; Goh, K.H.H.; Tan, Z.D.; Tan, S.T.M.; Tjiu, W.W.; Soh, J.Y.; Ng, Z.J.G.; Chan, Y.Z.; Hui, H.K.; Goh, K.E.J.: Electrically conductive filament for 3D-printed circuits and sensors, Applied Materials Today 9, 2017, pp. 167–175
[22] Landon, G.; Lewis, G.; Boden, G.F.: The influence of particle size on the tensile strength of particulate — filled polymers, Journal of Materials Science 12 (8), 1977, pp. 1605–1613
[23] Li, P.; Wang, Y.; Gupta, U.; Liu, J.; Zhang, L.; Du, D.; Foo, C.C.; Ouyang, J.; Zhu, J.: Transparent Soft Robots for Effective Camouflage, Advanced Functional Materials 29 (37), 2019, pp. 1901908
[24] Moiz, S.A.; Khan, I.A.; Younis, W.A.; Karimov, K.S.: Space Charge–Limited Current Model for Polymers, In: Yilmaz F. (Hrsg.): Conducting Polymers, InTech, 2016
[25] O'Halloran, A.; O'Malley, F.; McHugh, P.: A review on dielectric elastomer actuators, technology, applications, and challenges, Journal of Applied Physics 104 (7), 2008, pp. 71101
[26] Pejak Simunec, D.; Sola, A.: Emerging Research in Conductive Materials for Fused Filament Fabrication: A Critical Review, Advanced Engineering Materials, 2022, pp. 2101476
[27] Pelrine, R.; Kornbluh, R.; Pei; Joseph, J.: High-speed electrically actuated elastomers with strain greater than 100%, Science 287 (5454), 2000, pp. 836–839
[28] Rasmussen, L.: Electroactivity in Polymeric Materials, Springer US, Boston, MA, 2012
[29] Roldughin, V.; Vysotskii, V.: Percolation properties of metal-filled polymer films, structure and mechanisms of conductivity, Progress in Organic Coatings 39 (2-4), 2000, pp. 81–100
[30] Rosset, S.; Shea, H.R.: Flexible and stretchable electrodes for dielectric elastomer actuators, Applied Physics A 110 (2), 2013, pp. 281–307
[31] Rueda, M.M.; Auscher, M.-C.; Fulchiron, R.; Périé, T.; Martin, G.; Sonntag, P.; Cassagnau, P.: Rheology and applications of highly filled polymers: A review of current understanding, Progress in Polymer Science 66, 2017, pp. 22–53
[32] Scholz, G.; Gehringer, M.: Thermoplastische Elastomere, Im Blickfang, De Gruyter STEM, De Gruyter, Berlin, Boston, 2021
[33] Schoßig, M.: Bewertung der Schädigungsmechanismen von kurzglasfaserverstärkten Polyolefinen durch simultane Aufzeichnung der Schallemissionen unter quasistatischer und dynamischer Beanspruchung, 2010
[34] Shian, S.; Bertoldi, K.; Clarke, D.R.: Dielectric Elastomer Based "Grippers" for Soft Robotics, Advanced Materials 27 (43), 2015, pp. 6814–6819
[35] Spoerk, M.; Arbeiter, F.; Raguž, I.; Weingrill, G.; Fischinger, T.; Traxler, G.; Schuschnigg, S.; Cardon, L.; Holzer, C.: Polypropylene Filled With Glass Spheres in Extrusion-Based Additive Manufacturing: Effect of Filler Size and Printing Chamber Temperature, Macromolecular Materials and Engineering 303 (7), 2018, pp. 1800179
[36] Stano, G.; Di Nisio, A.; Lanzolla, A.M.; Ragolia, M.; Percoco, G.: Fused filament fabrication of commercial conductive filaments: experimental study on the process parameters aimed at the minimization, repeatability and thermal characterization of electrical resistance, The International Journal of Advanced Manufacturing Technology 111 (9-10), 2020, pp. 2971–2986

[37] Thomas, J.; Gemming, T.: Analytische Transmissionselektronenmikroskopie, Springer Vienna, Vienna, 2013
[38] Wu, J.-T.; Lien-Chung Hsu, S.; Tsai, M.-H.; Liu, Y.-F.; Hwang, W.-S.: Direct ink-jet printing of silver nitrate–silver nanowire hybrid inks to fabricate silver conductive lines, Journal of Materials Chemistry 22 (31), 2012, pp. 15599
[39] Zhang, W.; Dehghani-Sanij, A.A.; Blackburn, R.S.: Carbon based conductive polymer composites, Journal of Materials Science 42 (10), 2007, pp. 3408–3418
[40] Zhang, Y.; Ellingford, C.; Zhang, R.; Roscow, J.; Hopkins, M.; Keogh, P.; McNally, T.; Bowen, C.; Wan, C.: Electrical and Mechanical Self‐Healing in High‐Performance Dielectric Elastomer Actuator Materials, Advanced Functional Materials 29 (15), 2019, pp. 1808431

7 List of tables and figures

7.1 Tables

7.2 Figures

8 Abbreviations

AM	Additive Manufacturing
BSE	Backscattered Electrons
CPC	Conductive Polymer Compound
CB	Carbon Black
CF	Carbon Fibre
DEA	Dielectric Elastomer Actuator
FFF	Fused Filament Fabrication
GS	Glass Spheres
MEX	Material Extrusion
R_V	Variable Resistance
SCLC	Space Charge Limited Current
SE	Secondary Electrons
SEM	Scattering Electron Beam Microscope
s_z	strain of actuator
t	exponent dependent on aspect ratio
TPE	thermoplastic elastomer
TPU	thermoplastic polyurethane
V	Voltage
Y	Young's Modulus
Z	thickness of membrane
Φ	filler volume fraction
φ_c	percolation threshold
ε_0	vacuum permittivity
ε_r	relative permittivity
σ_c	conductivity of CPC
σ_f	conductivity of filler

9 Appendix

9.1 Fillers and Matrix

Elastollan® 1170 A

Thermoplastic Polyurethane Elastomer (Polyether)

BASF Polyurethanes GmbH

PROSPECTOR®
www.ulprospector.com

Technical Data

Product Description			
Thermoplastic Polyether Polyurethane Elastomers with outstanding hydrolysis resistance, low temperature flexibility and resistance to micro-organisms.			
Typical applications Cable jackets, plugs and terminations, spiral tubing, Films, ski-boot shells, ear tags, technical mouldings like mining screens, railway pads, seals.			
General			
Material Status	• Commercial: Active		
Literature [1]	• Processing - Elastollan (English) • Technical Datasheet (English)		
Search for UL Yellow Card	• BASF Polyurethanes GmbH • Elastollan®		
Availability	• Europe		
Features	• Hydrolysis Resistant	• Low Temperature Flexibility	• Microbe Resistant
Uses	• Cable Jacketing • Film • Mining Applications	• Molded Ear Tags • Plugs • Seals	• Sporting Goods • Tubing
Processing Method	• Blow Molding	• Extrusion	• Injection Molding

Physical	Nominal Value Unit	Test Method
Density	1.08 g/cm³	ISO 1183/A
Mechanical	**Nominal Value Unit**	**Test Method**
Abrasion Loss	< 50.0 mm³	ISO 4649-A
Elastomers	**Nominal Value Unit**	**Test Method**
Tensile Stress		DIN 53504
20% Strain	1.30 MPa	
100% Strain	2.00 MPa	
300% Strain	4.80 MPa	
Tensile Stress (Yield)	30.0 MPa	DIN 53504
Tensile Elongation (Break)	850 %	DIN 53504
Tear Strength [3]	44 kN/m	ISO 34-1
Compression Set		ISO 815
23°C, 72 hr	24 %	
70°C, 24 hr	50 %	
Impact	**Nominal Value Unit**	**Test Method**
Charpy Notched Impact Strength		ISO 179
-30°C	No Break	
23°C	No Break	
Hardness	**Nominal Value Unit**	**Test Method**
Shore Hardness (Shore A, 3 sec)	71	ISO 7619

Injection	Nominal Value Unit
Processing (Melt) Temp	170 to 240 °C
Mold Temperature	20.0 to 70.0 °C
Extrusion	**Nominal Value Unit**
Melt Temperature	160 to 220 °C

Figure 45: Technical data sheet from Elastollan® 1170 A from BASF

• Ag/Carbon fiber 30/30 fi

Silver coated carbon fibers

• Typical Properties:

Apparent density:		0,2 – 0,4 g/cm³
PSD (Laser)	D10:	6 – 12 µm
	D50:	25 – 35 µm
	D90:	130 – 170 µm
Average fiber length:		80µm
Average diameter:		7µm
Ag-content:		28,0 – 32,0 %
Powder resistivity:		1,6 mΩ (typical)

• Typical PSD curve (PSD for fibers by laser is critical)

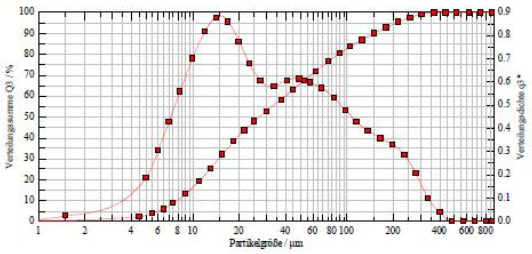

Other Ag-content, other PSD, organic coating: available on request

• SEM picture

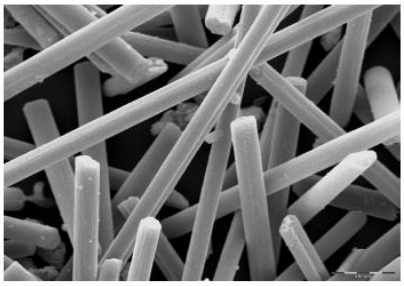

• SEM picture

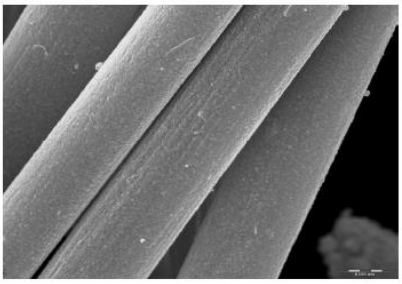

Figure 46: Technical data sheet of silver coated carbon fibres

• Ag/glass 5/25 s

Silver coated glass spheres

• Typical Properties:

Apparent density:		0,80 – 1,20 g/cm³
PSD (Laser)	D10:	3 – 7 µm
	D50:	5 – 10 µm
	D90:	13 – 18 µm
Ag-content:		23 – 26 %
Powder resistivity:		1,0 mΩ (typical)

• Typical PSD curve

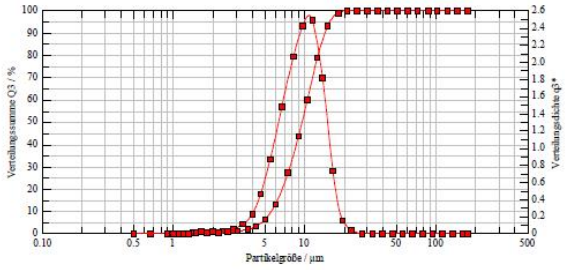

Other Ag-content, other PSD, organic coating: available on request

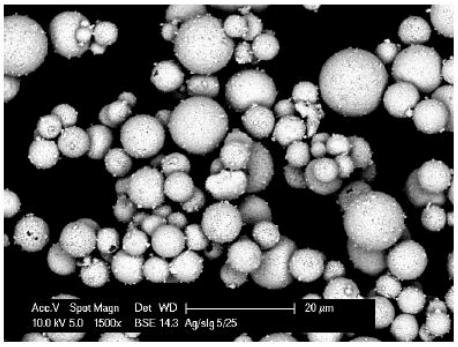

• SEM picture

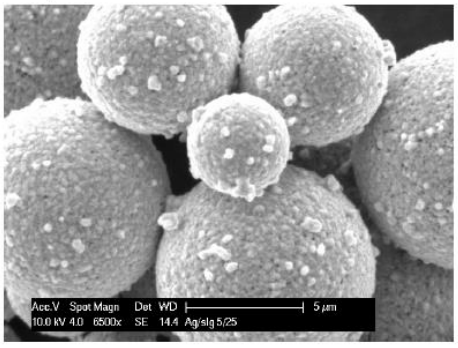

Figure 47: Technical data sheet of silver coated glass spheres (5 µm)

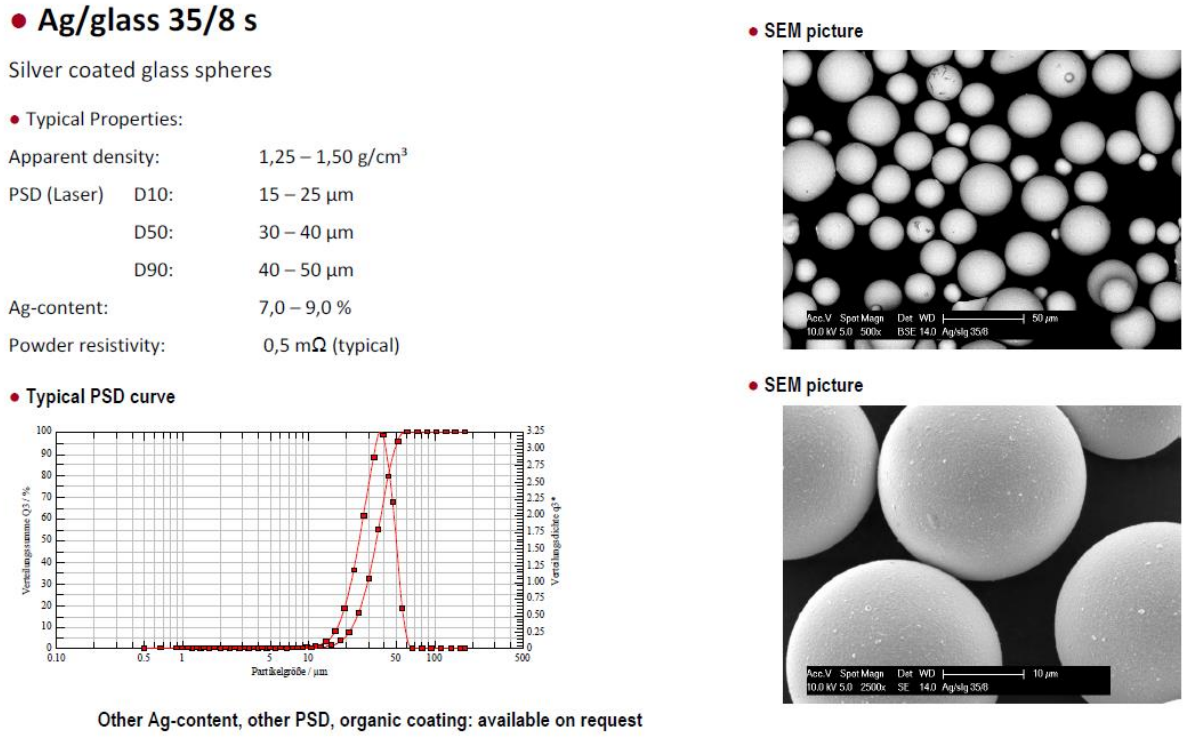

Figure 48: Technical data sheet of silver coated glass spheres (35 µm)

9.2 Kneading

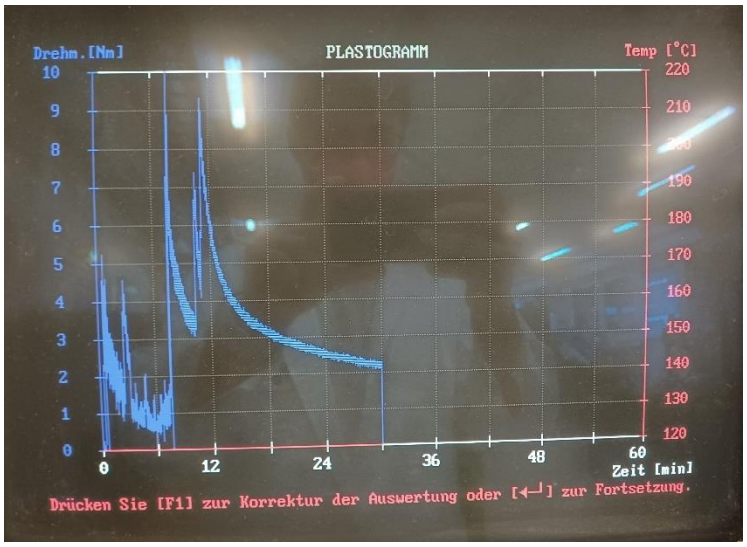

Figure 49: Kneading process of CPC_CF_10-vol.%

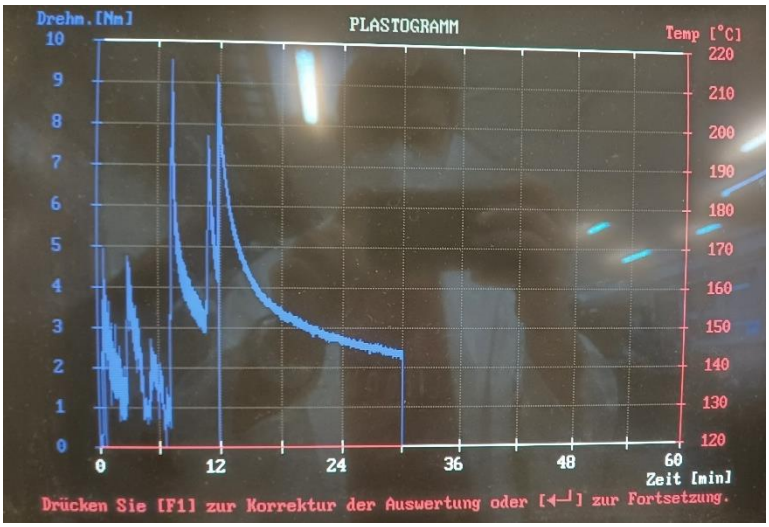

Figure 50: Kneading process of CPC_CF_12,5-vol.%

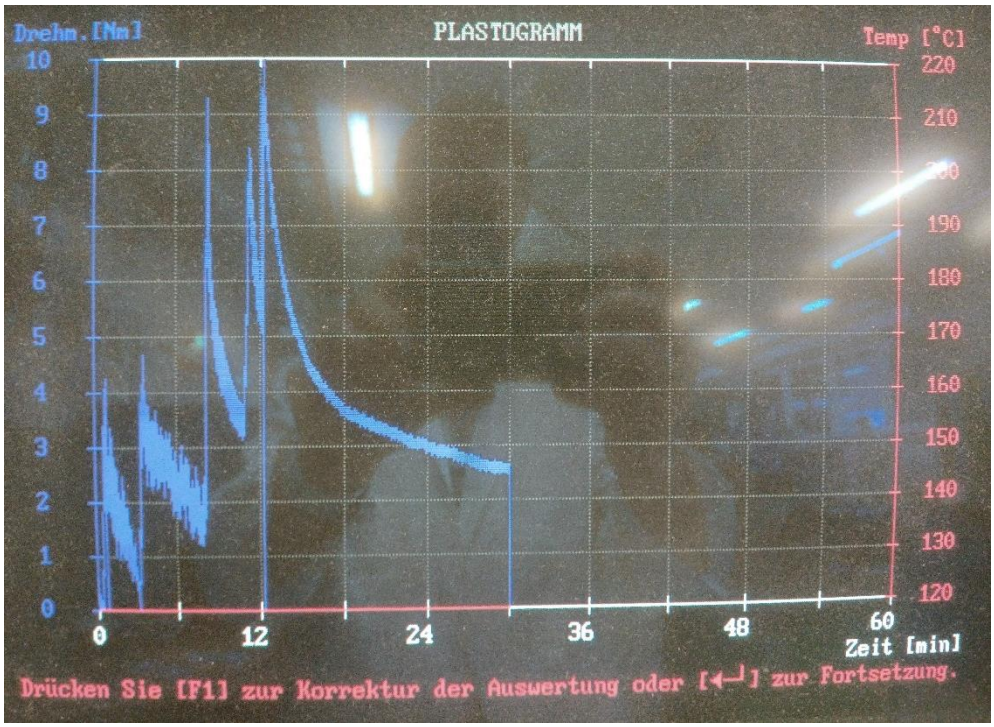

Figure 51: Kneading process of CPC_CF_15-vol.%

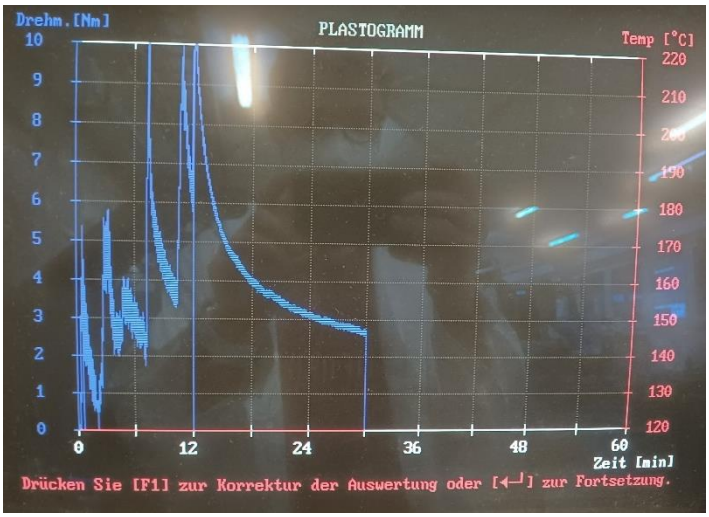

Figure 52: Kneading process of CPC_CF_17,5-vol.%

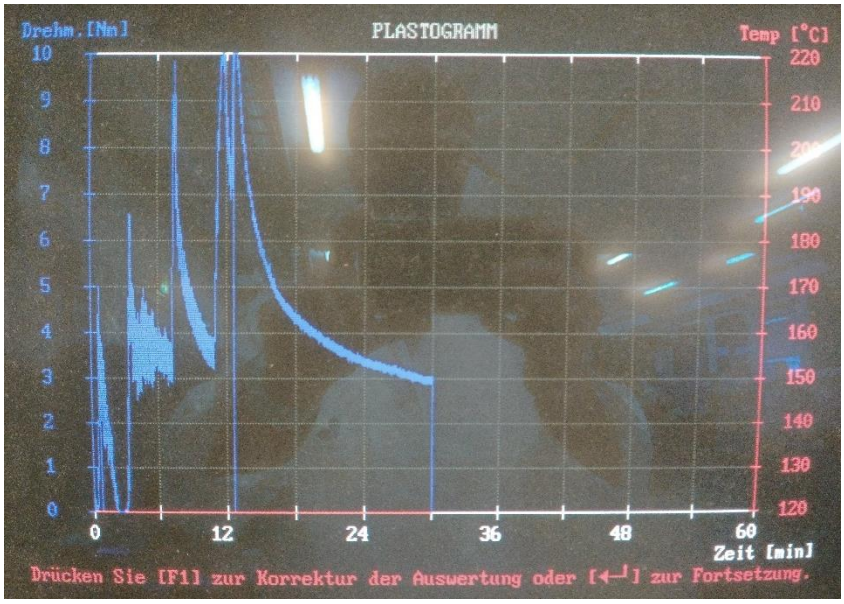

Figure 53: Kneading process of CPC_CF_20-vol.%

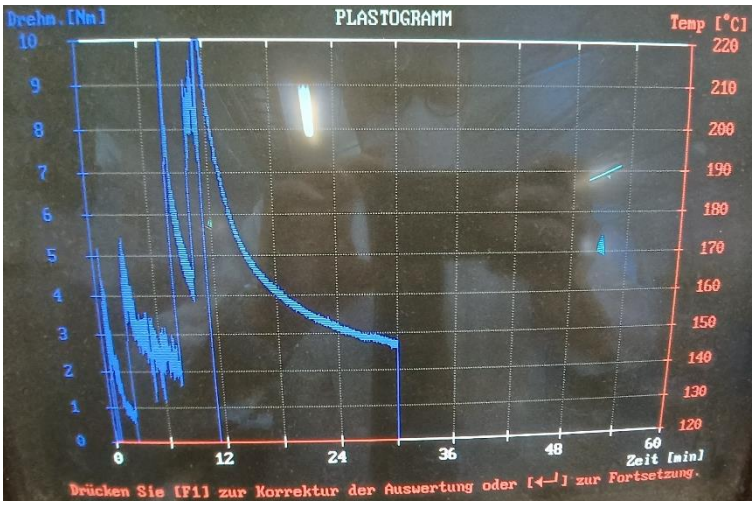

Figure 54: Kneading process of CPC_CF_15-vol.%_GS_5/25_2,5-vol.%

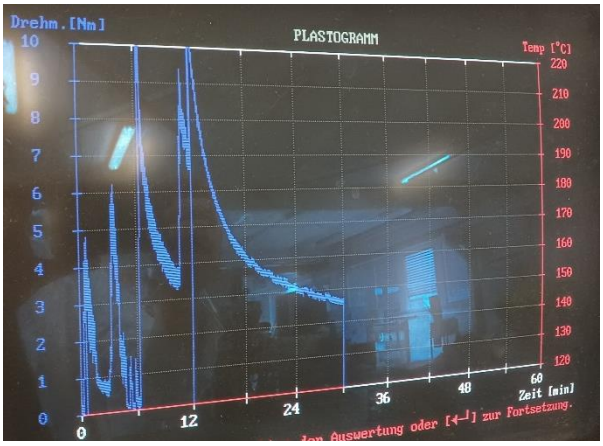

Figure 55: Kneading process of CPC_CF_15-vol.%_GS_5/25_5-vol.%

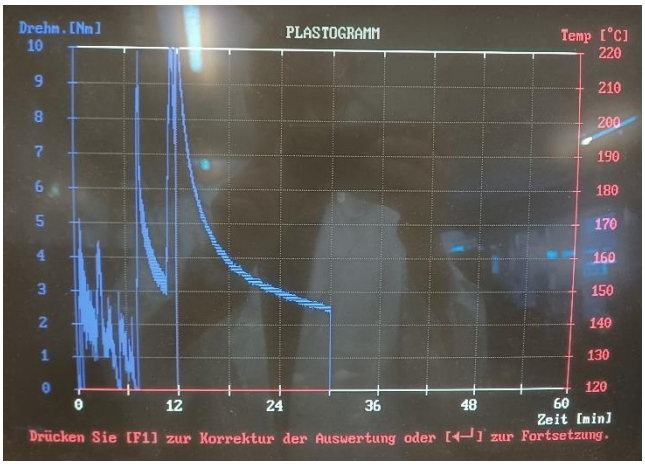

Figure 56: Kneading process of CPC_CF_15-vol.%_GS_35/8_2,5-vol.%

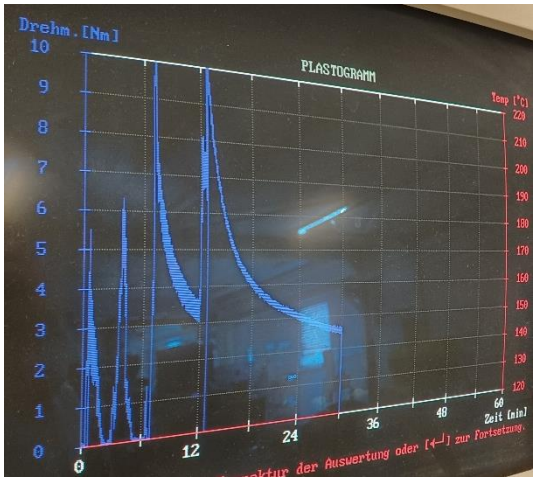

Figure 57: Kneading process of CPC_CF_15-vol.%_GS_35/8_5-vol.%

9.3 High Pressure Capillary Rheometer

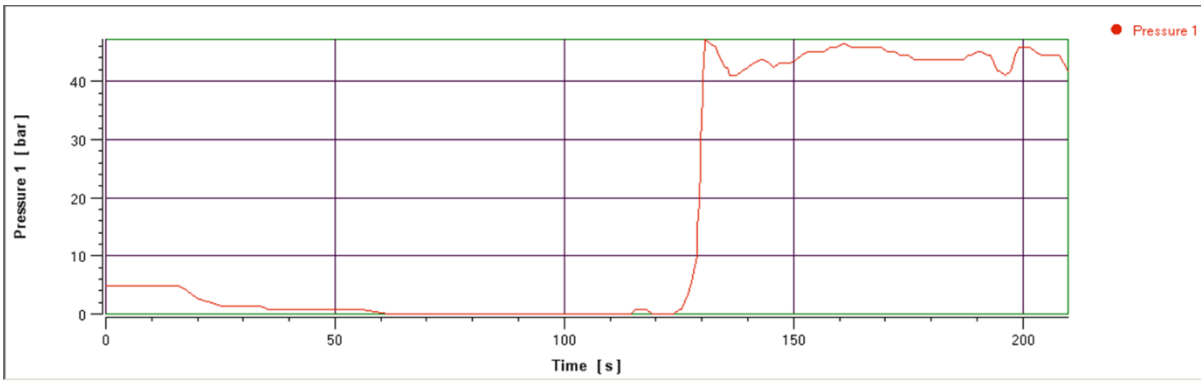

Figure 58: HPCR process of CPC_CF_10-vol.%

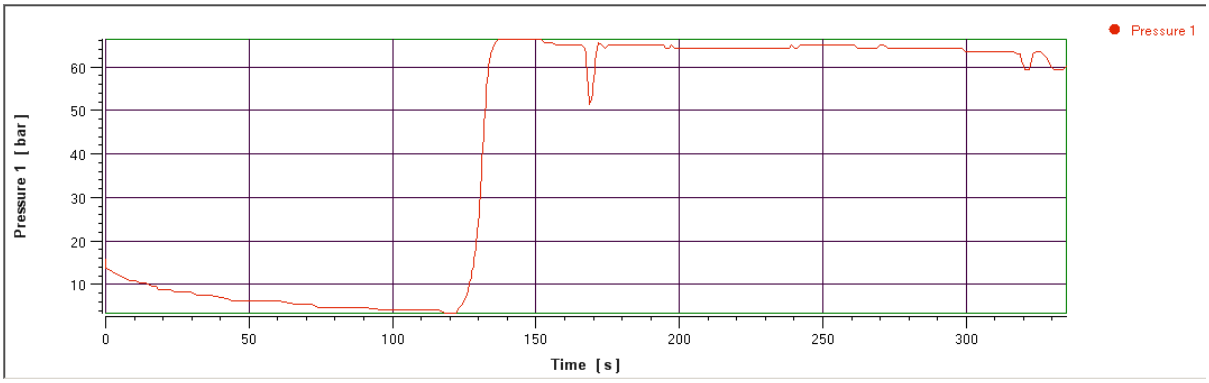

Figure 59: HPCR process of CPC_CF_12,5-vol.%

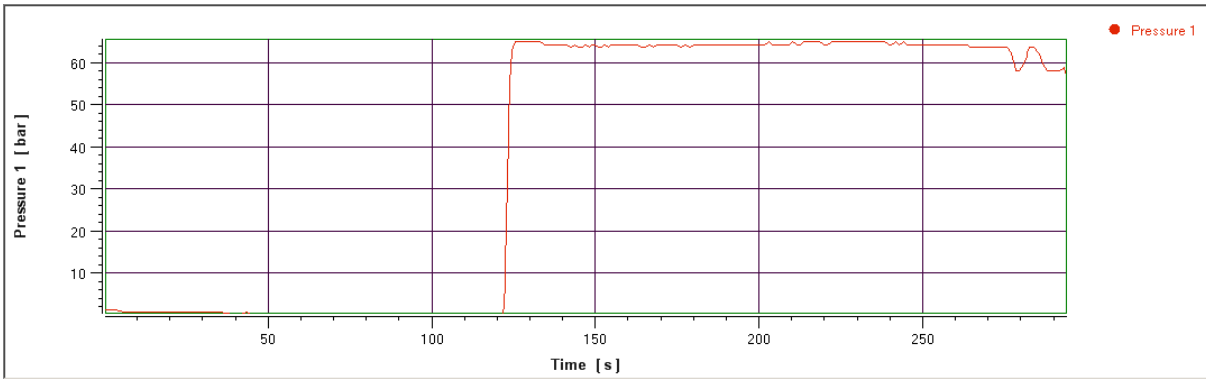

Figure 60: HPCR process of CPC_CF_15-vol.%

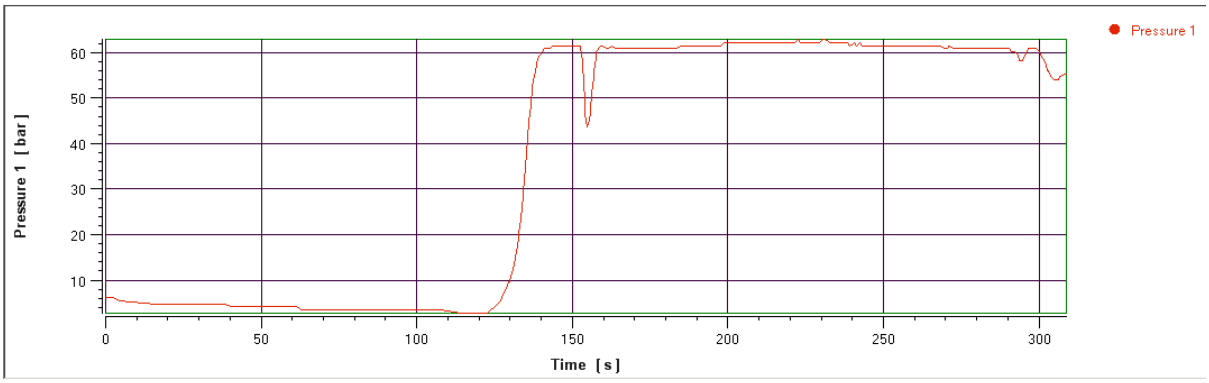

Figure 61: HPCR process of CPC_CF_17,5-vol.%

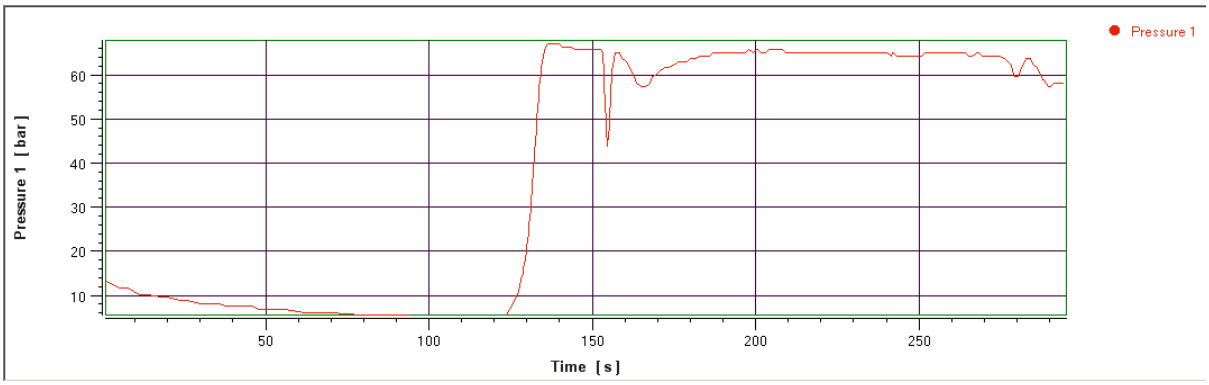

Figure 62: HPCR process of CPC_CF_20-vol.%

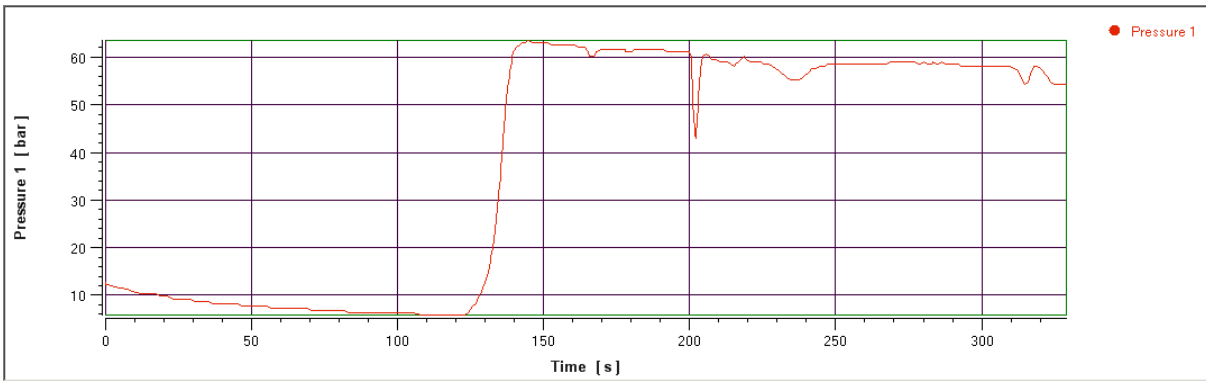

Figure 63: HPCR process of CPC_CF_15-vol.%_GS_5/25_2,5-vol.%

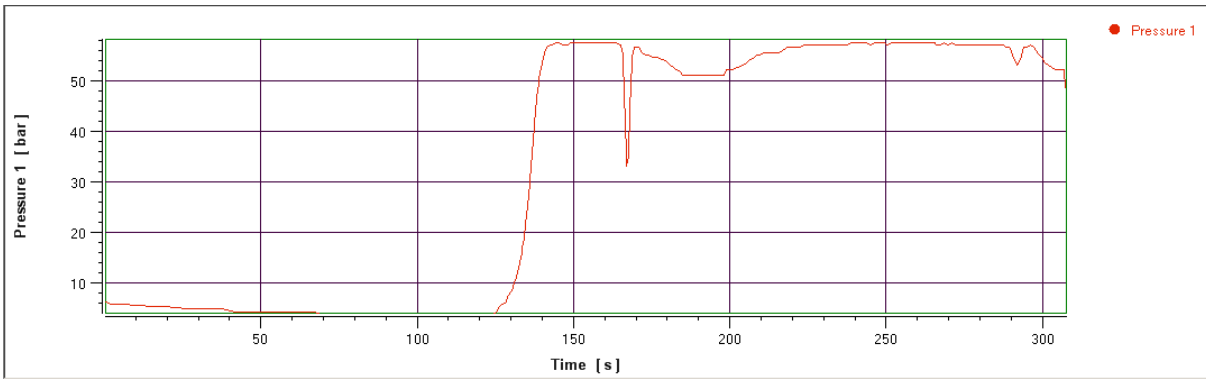

Figure 64: HPCR process of CPC_CF_15-vol.%_GS_5/25_5-vol.%

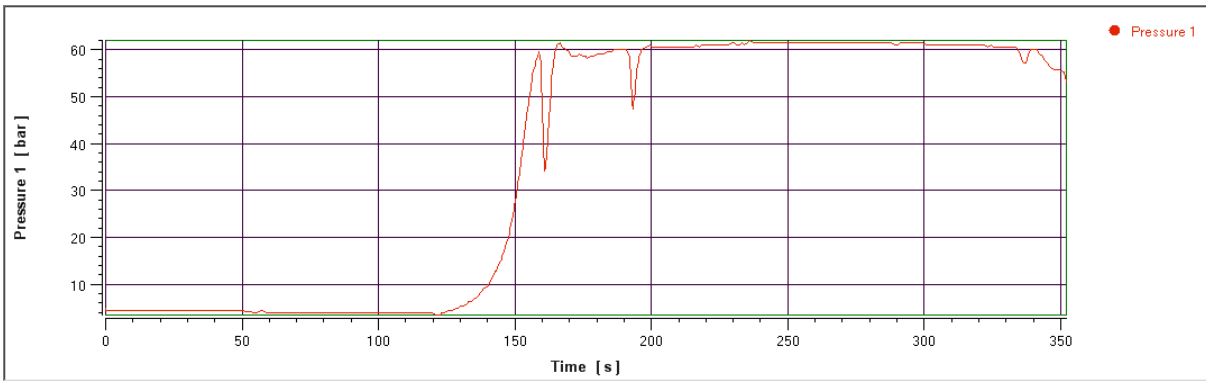

Figure 65: HPCR process of CPC_CF_15-vol.%_GS_35/8_2,5-vol.%

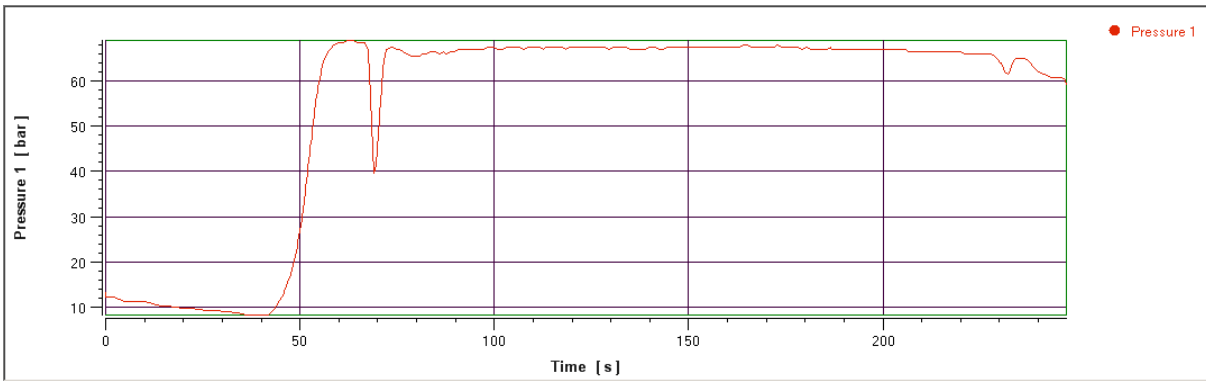

Figure 66: HPCR process of CPC_CF_15-vol.%_GS_35/8_5-vol.%